minerals

MDPI

Review

Antimony's Significance as a Critical Metal: The Global Perspective and the Greek Deposits

Christos Kanellopoulos [1,2,*], Sotiris Sboras [3], Panagiotis Voudouris [1], Konstantinos Soukis [1] and Robert Moritz [2]

1 Faculty of Geology and Geoenvironment, National and Kapodistrian University of Athens, Panepistimiopolis, Zografou, 15784 Athens, Greece; voudouris@geol.uoa.gr (P.V.); soukis@geol.uoa.gr (K.S.)
2 Department of Earth Sciences, University of Geneva, Rue des Maraîchers 13, 1205 Geneva, Switzerland; robert.moritz@unige.ch
3 Institute of Geodynamics, National Observatory of Athens, Lofos Nymphon, Thesio, 11810 Athens, Greece; sboras@noa.gr
* Correspondence: ckanellopoulos@gmail.com

Abstract: Antimony is widely acknowledged as a critical raw material of worldwide significance, based on its recognition by many countries. According to current projections, there is an anticipated increase in the demand for antimony in the forthcoming years. An issue of significant concern within the supply chain, which poses a substantial obstacle to sustainable development, is the global unequal allocation of abundant antimony resources. Most nations exhibited a high degree of dependence on a few countries for their net imports of antimony, resulting in a notable disruption and raising concerns regarding the supply chain. In most countries, antimony exploration and exploitation have been paused for a long period due to financial constraints associated with operations and environmental concerns. Nowadays, identifying additional antimony reserves, particularly in countries that heavily rely on new technologies and use significant amounts of antimony, is imperative and presents a pressing endeavor. Greece is recognized as one of the European Union member states with identified antimony deposits and a historical record of antimony exploitation. A thorough description, examination, and re-assessment of all existing data on the deposits and occurrences of antimony in Greece is presented. Most of Greece's antimony deposits are related to hydrothermal processes, controlled by specific tectonic structures, and associated with Cenozoic magmatism. They are classified either as simple Sb-deposits, where the primary ore is a stibnite mineral, or complex polymetallic deposits with varying contents that include antimony minerals.

Keywords: antimony (Sb); stibnite; critical metal; sustainable development; tectonic control metal cycling; ore deposits

check for updates

Citation: Kanellopoulos, C.; Sboras, S.; Voudouris, P.; Soukis, K.; Moritz, R. Antimony's Significance as a Critical Metal: The Global Perspective and the Greek Deposits. *Minerals* **2024**, *14*, 121. https://doi.org/10.3390/min14020121

Academic Editors: Jaroslav Dostal, Martiya Sadeghi and David Lentz

Received: 17 December 2023
Revised: 15 January 2024
Accepted: 22 January 2024
Published: 23 January 2024

Copyright: © 2024 by the authors. Licensee MDPI, Basel, Switzerland. This article is an open access article distributed under the terms and conditions of the Creative Commons Attribution (CC BY) license (https://creativecommons.org/licenses/by/4.0/).

1. Introduction

Antimony (Sb) is considered to be a critical raw material (CRM) of global significance, as acknowledged by multiple countries and unions, including the European Union [1], the United States of America [2], China [3], the United Kingdom [4], and Canada [5]. Antimony has been recognized as a CRM since its inclusion in the first European Union (EU) CRM report published by the European Commission in 2010 [6]. Despite this, the EU and many of the countries cited above do not extract antimony ores inside their territorial boundaries and are entirely dependent on imports.

Antimony has a strong affinity with sulfur; thereby, it is classified as a chalcophile element. Moreover, it is often seen to create chemical compounds with a range of metallic elements, leading to the formation of sulfosalts [7]. Although it is relatively uncommon in the Earth's upper crust, with a concentration of 0.4 ppm [8], it exhibits similarities to certain other heavy rare-earth elements [9]. Antimony is often encountered in elevated concentrations at specific ore deposits. Antimony is widely acknowledged as a significant

pathfinder element in the context of geochemical prospecting surveys, primarily owing to its strong association with various mineral occurrences [10].

Antimony has several applications in the industrial sector, such as in the realms of green energy and emerging technologies. The use of emerging technologies in developing high-capacity storage batteries highlights the significance of antimony as a CRM in facilitating the move toward sustainable development and energy transition [11]. The present projections for future antimony demand exhibit variability. Mordor Intelligence [12] predicts that the antimony market will have a yearly growth rate of 5% until 2026. Perpetua Resources [13] asserts that an extra annual production of 18 kt (equivalent to 12% of the 2018 production) will be necessary until the year 2030. Over 60% of the global supply originates from China, which can cause a significant supply disruptions and concern [11].

The nations at the forefront of new technology and manufacturing, such as the USA and the EU, must decrease their reliance on imports. Additionally, both the USA and EU own various antimony deposits that have the potential for development and processing. In addition to the emergence of novel primary sources, secondary sources have the potential to provide substantial quantities of antimony, i.e., recycling of lead–acid batteries [11].

The significance of antimony as a critical raw material is unquestionable, and the substantial potential for supply chain disruptions is a significant reason for worry. Hence, the re-assessment and redefinition of occurrences and deposits have high significance. In the EU, one of the countries with antimony deposits/occurrences is Greece. Although antimony deposits/occurrences were identified in the last few decades, only a few studies have been carried out until now. The aims of this study were twofold: (i) to provide an up-to-date overview of the worldwide perspective and applications of antimony as a certified reference material, and (ii) to thoroughly examine and re-evaluate all existing data on the deposits and occurrences of antimony in Greece.

2. Global Perspective

2.1. World Resources, Production and Perspectives

The distribution of antimony deposits is only located within a geographically restricted area. China and Russia, and their respective political and economic partners, have substantial influence over the worldwide antimony upstream supply chain (Figures 1 and 2). According to the United States Geological Survey's (USGS) estimate in 2021, these businesses jointly represent over 90% of the global mining production of antimony [13].

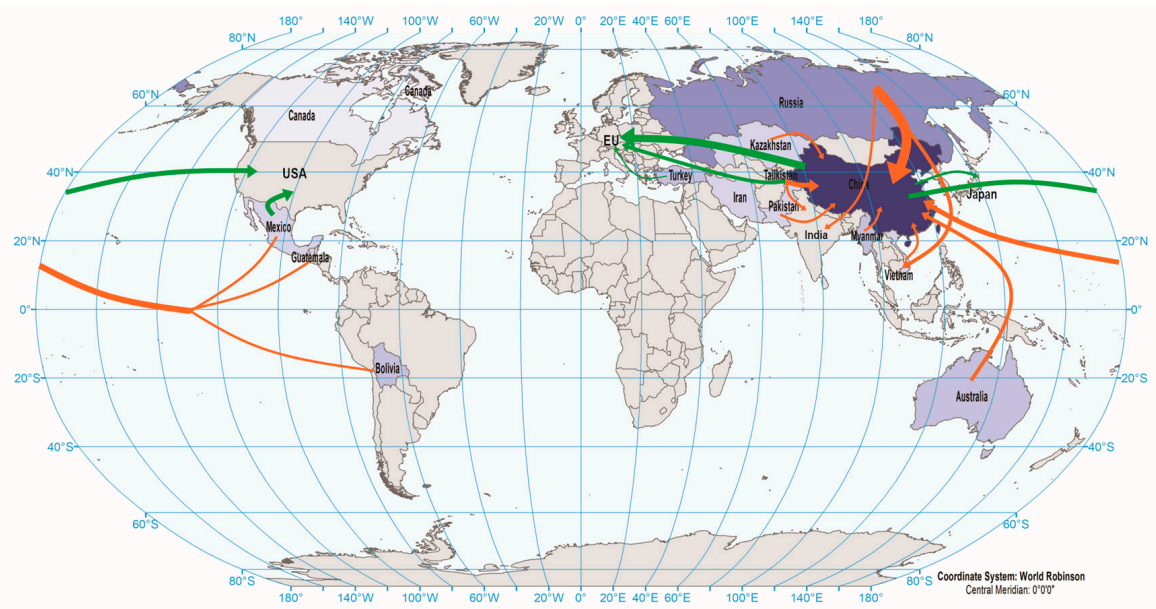

Figure 1. Map of the major antimony supply chain dynamics (orange arrows: Sb ores (include all types), green arrows: Sb products exports; from (based on [11,14]).

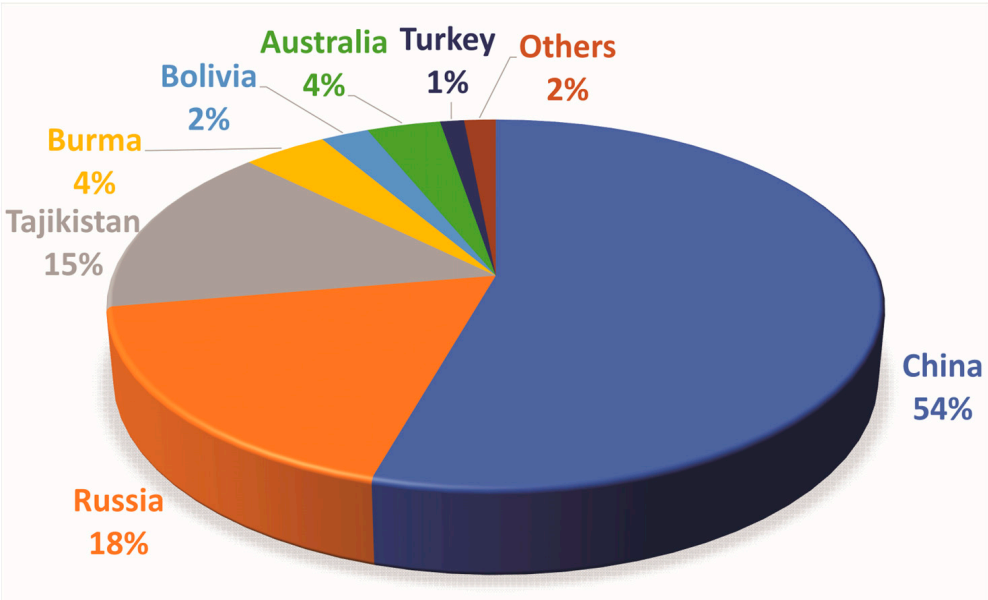

Figure 2. Distribution of Global Mine Production of Antimony (2022) (based on [15]).

In the year 2010, the Chinese government introduced two policies that led to a reduction in domestic antimony production, causing significant disruption in the markets. At the beginning of 2010, the Chinese government expressed its disinclination to provide authorization for any prospective antimony initiatives until the culmination of 30 June 2011. During a similar timeframe, the Chinese government enforced the shutdown of around 100 antimony smelters in its main antimony-producing region. The implementation of this action was carried out with the objective of ceasing unauthorized mining activities and minimizing the adverse effects on the environment [3,16].

Until 2021, China retained its status as the primary global producer of antimony, accounting for 55% of the total global mining production. Russia and Tajikistan also contributed, constituting 23% and 12% of the total, respectively [17]. In 2021, the global supply of antimony raw materials and the subsequent production of antimony products faced constraints as a result of environmental audits carried out in China and temporary mine closures implemented to mitigate the global transmission of the COVID-19 pandemic. The limited availability of raw materials, coupled with difficulties in worldwide transportation, led to a reduced supply of processed antimony in the market. As a result, there was a notable escalation in the price of antimony, reaching $6.65 per pound in October 2021, which marked a substantial rise compared to the average annual price of $2.67 per pound in 2020 [17].

Between 2012 and 2016, the European Union (EU) maintained a stable average importation of 22,200 tons per year of antimony metal and antimony oxides. China is the primary source of imports for the European Union, accounting for ca. 40% of the EU's overall imports, with an annual import volume of 17,650 tons [18].

According to Laznicka [19,20] the global collection of 24 giant antimony deposits included a cumulative quantity of 6.97 million metric tons of antimony. According to Laznicka's estimation, the overall world endowment of antimony is projected to range from 7.1 to 7.5 million metric tons [3]. The most significant reserves are located in China, Russia, Bolivia, Mexico, USA, South Africa, and Tajikistan. Approximately one-third of these deposits are found in China [3,21].

There are several known antimony resources which are mainly unevenly distributed over the planet. In the current market situation, there is a preference for exploiting only large deposits that are suitable for implementing high-volume bulk-mining techniques. The EU, the USA, and the other countries in the Western Hemisphere have antimony resources inside their territorial boundaries, but they are not ample resources [3]. For example,

antimony resources are found in six European nations, i.e., France, Germany, Sweden, Finland, Slovakia, and Greece. An additional problem is that the majority of resources in Europe rely on historical estimations, and their economic significance at present is questionable [18].

The potential future mining of antimony resources is expected to mostly include either simple stibnite or precious metal deposits associated with copper, lead, and/or zinc. Also, gold is a significant co-product of antimony. However, it is often the primary focus of extraction in gold–antimony vein mining operations. The inclusion of antimony in gold ore poses challenges in terms of processing, leading to increased difficulty and cost. Consequently, it may be necessary to accumulate a quantity of gold ore with a significant antimony content [3,9]. In the future, the recovery of antimony from precious metal deposits might potentially serve as the most easily accessible source of antimony in the event of a sudden spike in demand [3].

In Greece, a member of the EU, the presence of antimony was identified in several locations and different geological settings, including cases of simple antimony deposits and cases of precious metal deposits. In some cases, antimony exploitation projects took place mainly in the first half of the last century. Proposing the feasibility of sustainable exploitation initiatives in the present day.

2.2. Antimony Uses, Substitution, Recycling and Environmental Considerations

Antimony is categorized as a metalloid due to its chemical characteristics. According to Miller [7], antimony demonstrates brittleness when used as an independent material. However, when integrated into alloys, it provides improved strength, hardness, and corrosion resistance. The material has a low level of thermal and electrical conductivity. The natural abundance of this metal is limited, owing to its strong affinity for sulfur and other metals, including lead, copper, and silver [22].

Antimony has played a significant role as an element of great importance throughout human history. As early as around 3100 B.C., stibnite (Sb_2S_3), the primary ore mineral for antimony, was employed by the ancient Egyptians and early Hindus to produce black eye makeup [3]. The initial application of antimony in the field of technology was primarily associated with the advancement of cast metal printing types, mirrors, bell metal, and pigments. During the 18th century, France, Germany, and Italy emerged as the primary nations engaged in antimony production. The greater utilization of storage batteries in automobiles throughout the 1930s led to a significant rise in the demand for antimony. During the 1940s, the demand for antimony experienced a significant increase due to its numerous military uses in World War II [7]. The global mining output saw substantial growth from 1900 to 2016, with a rise from 7710 metric tons to 186,000 metric tons [23].

Nowadays, antimony is predominantly utilized as a flame retardant and in lead–acid storage batteries designed for automotive applications. The batteries comprise a lead alloy containing around 4%–6% antimony. It has been shown that including antimony in the alloy contributes to increased resistance [24]. Metallurgical antimony is predominantly utilized in lead–acid storage batteries, constituting almost 66% of its overall usage [3].

According to Tercero Espinoza et al. [25], substituting antimony in specific applications is relatively easy. Other elements have the potential to serve as substitutes for antimony compounds in various applications. Calcium, copper, selenium, strontium, sulfur, and tin have been identified as potential alternatives to antimony for strengthening lead and replacing antimony in lead–acid batteries. It is worth noting that these substitutes have demonstrated improved performance in certain cases [9]. The implementation of substitutes may necessitate modifications in manufacturing procedures and industrial equipment. However, it is important to note that these substitutes have their own supply challenges and may incur higher costs.

Antimony recovery through recycling has been achieved in certain cases, especially in specific applications where it is employed as an addition in lead alloys. Most secondary antimony metal, i.e., recovered after recycling, is derived from the recycling of lead–acid

batteries, which typically contain a Sb content ranging from 0.6% to 1.5% [22]. Secondary antimony plays a substantial role in the supply chain of several nations, constituting around 20% of the overall antimony utilized and amounting to an annual production of over 40,000 tons [22,26].

Antimony mining and refining processes give rise to significant environmental concerns since, in humans, antimony has been associated with many disorders affecting the liver, pulmonary, and cardiovascular systems, as well as the skin [27]. The Rish [28] and Seal et al. [3] studies present a thorough review of the environmental considerations concerning antimony. Presently, there is a lack of comprehensive environmental studies concerning case studies that examine the behavior of antimony and associated trace elements in a modern mining environment [3]. The environmental concern of the local communities is one of the main reasons for the cancellation of mining projects, especially in developed countries. It is of great importance that we conduct comprehensive environmental studies in antimony-mining areas. A comprehensive understanding of the environment and a strong commitment to environmental conservation, coupled with a sense of social responsibility, are essential in any undertaking involving the exploitation of antimony in order to attain widespread support within society.

2.3. Characteristics and Classifications of Antimony Deposits

Antimony occurs in many ore deposits in diverse geological settings, types, and ages. However, it is important to acknowledge that the occurrence of elevated concentrations of antimony in ores is infrequent, and the presence of economically exploited stibnite deposits is generally constrained by restricted size and sporadic features (Figure 3) [22]. Usually, these types of deposits are associated with hydrothermal processes [29] and, in several cases, are tectonically controlled. The deposits that produce antimony can be classified into two primary categories based on their metal and mineral composition: (i) deposits primarily consisting of simple stibnite, where antimony is the main commodity extracted during mining operations, and (ii) complex polymetallic deposits containing varying amounts of different elements, where antimony is obtained as a byproduct of mining for other commodities [3,22]. According to Schwarz-Schampera [22], these types of antimony deposit can be distinguished based on fluid generation and metal source into: (i) low-temperature hydrothermal (epithermal) origin in shallow crustal environments associated with magmatic fluids, (ii) metamorphogenic hydrothermal origin in consolidated crustal environments derived from crustal fluids, triggered by, and with contributions from, magmatic heat and expelled fluids; and (iii) reduced intrusion-related gold systems.

Antimony fissure-vein deposits can manifest in areas enclosed by extensive shear zones and strike-slip fault zones [3]. According to the study conducted by Pitcairn et al. [30], it was suggested that high-grade metamorphism, distinguished by temperatures over 400 °C, can facilitate the mobilization of antimony and its subsequent transportation by hydrothermal fluids. Under certain conditions, these fluids may subsequently lead to the development of quartz–antimony veins at lower temperatures. Most prominent quartz–stibnite deposits exhibit distinct features, such as siliciclastic sedimentary host rocks and focused migration pathways for upward hydrothermal fluid circulation from deeper high-temperature crustal levels. The primary sources of present and recent mine production are the quartz–stibnite veins and replacement deposits. Various types of hydrothermal systems have the potential to give rise to these formations, such as the peripheral regions of orogenic gold deposits, intrusion-related gold deposits, porphyry copper and molybdenum deposits, polymetallic mesothermal vein deposits, and sediment-hosted Carlin-type gold deposits [31]. Additionally, they may be isolated without any discernible connection to other mineral deposits. Notable quartz–stibnite deposits of the utmost importance include the Kharma deposit (Bolivia), the Beaver Brook and Lake George deposits (Canada), the Xikuangshan deposit (China), the Sarylakh and Sentachan deposits (Russia), the Consolidated Murchison deposit (South Africa), and the Yellow Pine and U.S. Antimony Mine deposits in Montana (MT, USA) (Figure 3) [3].

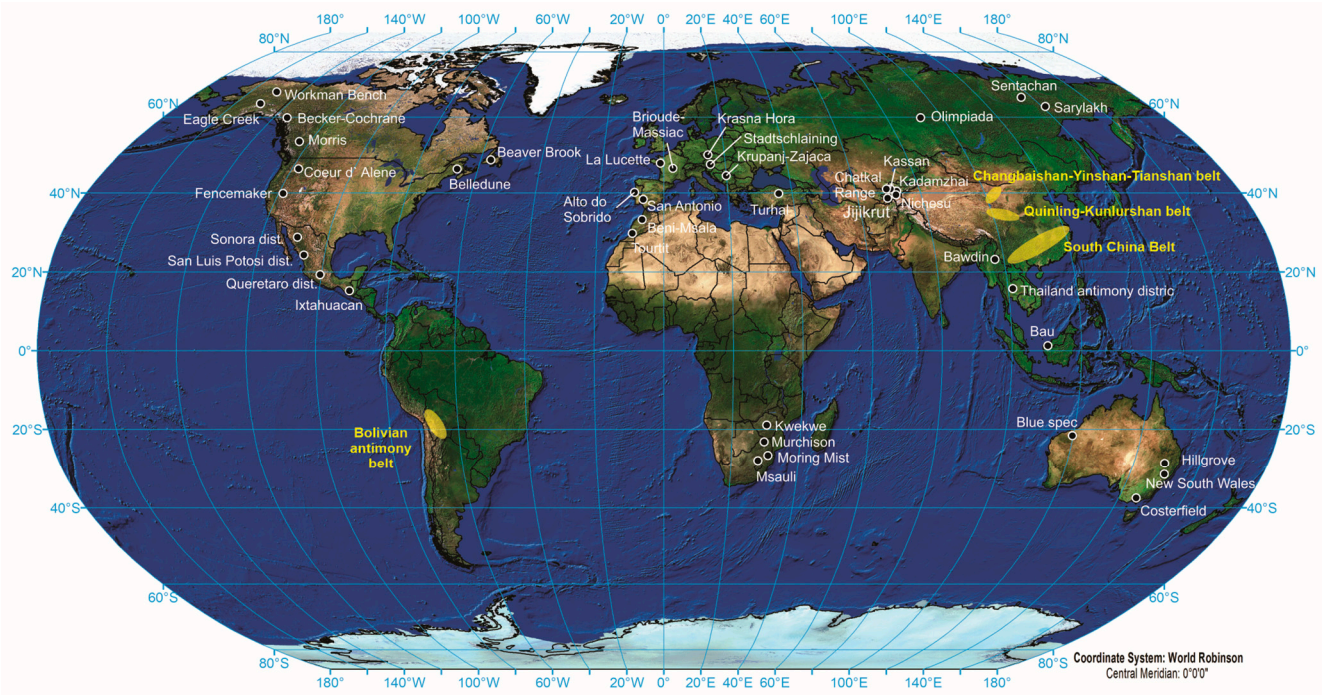

Figure 3. World map of the main antimony deposits, mines, and important occurrences worldwide. The symbols indicate either a single mine/deposit or a number of deposits (based on [3,22]).

There are many deposits, such as the Xikuangshan deposit (China), the Sentachan and Sarylakh (Russia), the Antimony Line deposit (South Africa), and the U.S. Antimony Mine in Montana (USA), that exhibit a connection with notable structural fault systems. These fault systems can facilitate the migration of deep regional metamorphic fluids. However, it is important to acknowledge that igneous heat sources associated with more confined fault and fracture zones have been detected at the deposits in Bolivia and the Lake George and Beaver Brook deposits (Canada) [3].

Antimony-bearing deposits are generally associated with calc-alkaline to peralkaline, porphyritic felsic to intermediate volcanic, and intrusive rocks in a volcanic cauldron setting. The host rocks exhibit varying hydrothermal alteration processes, including silicification, carbonatization, sericitization, chloritization, and greisenization. The primary volcanic host rocks consist of submarine, subaerial, and pyroclastic deposits, mostly composed of rhyodacite, dacite, and andesite. Intrusive host rocks range from subvolcanic to hypabyssal and consist of granite, granodiorite, quartz, and monzonite. Antimony deposits associated with intrusions, such as skarns, replacement ores, and vein-type deposits, occur near the magmatic source and are influenced by magmatic-hydrothermal processes. These deposits are generally found in plutons of various kinds, exhibiting features of I-, S-, and A-type granitoids [22,32].

Antimony occurs in a large variety of minerals, including sulfides, sulfosalts, oxides, antimonates, and antimonites [3,10]. The occurrence of antimony (Sb^0) in its original state is rare, mostly because of its high affinity for sulfur and other metals/metalloids, including cobalt, lead, bismuth, arsenic, and silver. Up to now, 264 unique mineral phases that include antimony have been documented [22]. A few of them have considerable economic importance as valuable sources of antimony. Several notable examples of minerals containing antimony include boulangerite ($Pb_5Sb_4S_{11}$), bournonite ($PbCuSbS_3$), gudmundite ($FeSbS$), jamesonite ($Pb_4FeSb_6S_{14}$), polybasite ($[(Ag,Cu)_6(Sb,As)_2S_7][Ag_9CuS_4]$), pyrargyrite ($Ag_3SbS_3$), tetrahedrite ($(Cu,Fe)_{12}Sb_4S_{13}$), and valentinite ($Sb_2O_3$) [7,9]. Pohl (2011) states that the Sb ore has the capacity to include deleterious elements, such as arsenic (As) and mercury (Hg). According to Pohl [33], stibnite (Sb_2S_3) is the most common and abundant Sb-ore-bearing mineral, typically found in association with small quantities of other metals

such as iron (Fe), cobalt (Co), lead (Pb), gold (Au), and silver (Ag). Based on Miller's [7] findings, it has been observed that the primary Sb ores generally consist of several metallic accessory minerals, including arsenopyrite, chalcopyrite, galena, gold, pyrite, pyrrhotite, sphalerite, and silver. Furthermore, the most prevalent gangue minerals included in these ores are quartz, calcite, and barite. The most regularly observed supergene antimony minerals are bindheimite ($Pb_2Sb_2O_6O$), kermesite (Sb_2S_2O), nadorite ($PbSbO_2Cl$), senarmontite (Sb_2O_3), and stibiconite ($Sb^{3+}Sb^{5+}{}_2O_6(OH)$) [3].

In conclusion, it can be said that enriched levels of antimony are mostly found in low-temperature magmatic-hydrothermal systems inside the epithermal environment. Antimony often demonstrates a tendency for enrichment in the distal segments of these geological systems, particularly at shallow depths and in close proximity to the Earth's surface. Also, it presents a strong correlation with hydrothermal silica and carbon dioxide, whereas the prevailing rock formation is generally carbonate, present either as sedimentary limestone or a notable hydrothermal alteration mineral phase [22].

3. Greek Antimony Deposits and Perspectives

In Greece, several antimony deposits have been identified (Figure 4) since the end of the previous century, and in some cases, exploitation projects have been undertaken.

Most Greek antimony deposits are associated with hydrothermal processes, influenced by tectonic structures, and are related to Cenozoic magmatism. Both simple stibnite deposits and complex polymetallic deposits with compositions of various elements, including antimony as a prominent metal constituent, occur. Moreover, antimony has been recognized as a minor mineral component in complex polymetallic deposits, rendering it unsuitable as a target for exploration efforts (Figure 4).

According to various researchers [34–37], the presence of Cu, Mo, W, Pb, Zn, Ag minerals in Cenozoic antimony deposits supports the hypothesis that they present geochemical affinities with Pb-Zn deposits of higher temperatures. Such occurrences are found in Greece (e.g., Kallintiri and parts of Philadelphia). In most metallogenetic provinces, Sb mineralization is a member of Pb-Zn hydrothermal systems, generally linked together by gradual transition. According to Mudrinic [36], Polymetallic antimony deposits (Sb-As + Pb-Zn) are formed at relatively high temperatures (160–330 °C) compared to monometallic Sb deposits or bimetallic Sb-As (90–200 °C).

The antimony deposits in Greece are located in central–eastern Macedonia and Thrace (i.e., Philadelphia, Lachanas-Rizana, Kallintiri, and Gerakario, NE Greece), on the Eastern Aegean Sea, i.e., Chios and Samos islands, and on Pelion Mountain (central Greece). These areas are located in the geotectonic zones of the Hellenic hinterland (Rhodope and Serbomacedonian massifs) and the internal Hellenides (Circum-Rhodope, Axios/Vardar and Pelagonian zones). The Hellenic hinterland belongs to the Cimmerian orogenic belt, formed in pre–late Jurassic times as a result of the collision between the northward-drifted Cimmerian continental fragments detached from Gondwana and Eurasia [38–44]. Compression of the Alpine orogenesis, which resulted in the westward stacking of the Hellenides, was followed by the late Eocene–lower Oligocene extension in northern Greece and later on in the central Aegean due to slab rollback and the retreat of the Hellenic Arc (also known as Hellenic Subduction Zone) resulting in the formation of upper-plate detachment faults and the exhumation of metamorphic core complexes (e.g., [45–58]). Various subsequent deformation stages are proposed, e.g., [59–63] until the lower-middle Pleistocene, which marks the beginning of the present-day stress field characterized by extension in most of the central northern Aegean, with the interference of the transcurrent North Anatolian Fault Zone's (NAFZ) shear in the north Aegean Sea and its two regional tectonic structures, i.e., the North Aegean Trough (NAT) and the North Aegean Basin (NAB) (e.g., [41,64–71]). The Aegean region is the locus of Cenozoic magmatism, with the volcanic activity migrating southwards from northern Greece since early Eocene times, associated with the southward migration of the Hellenic Arc [72–76].

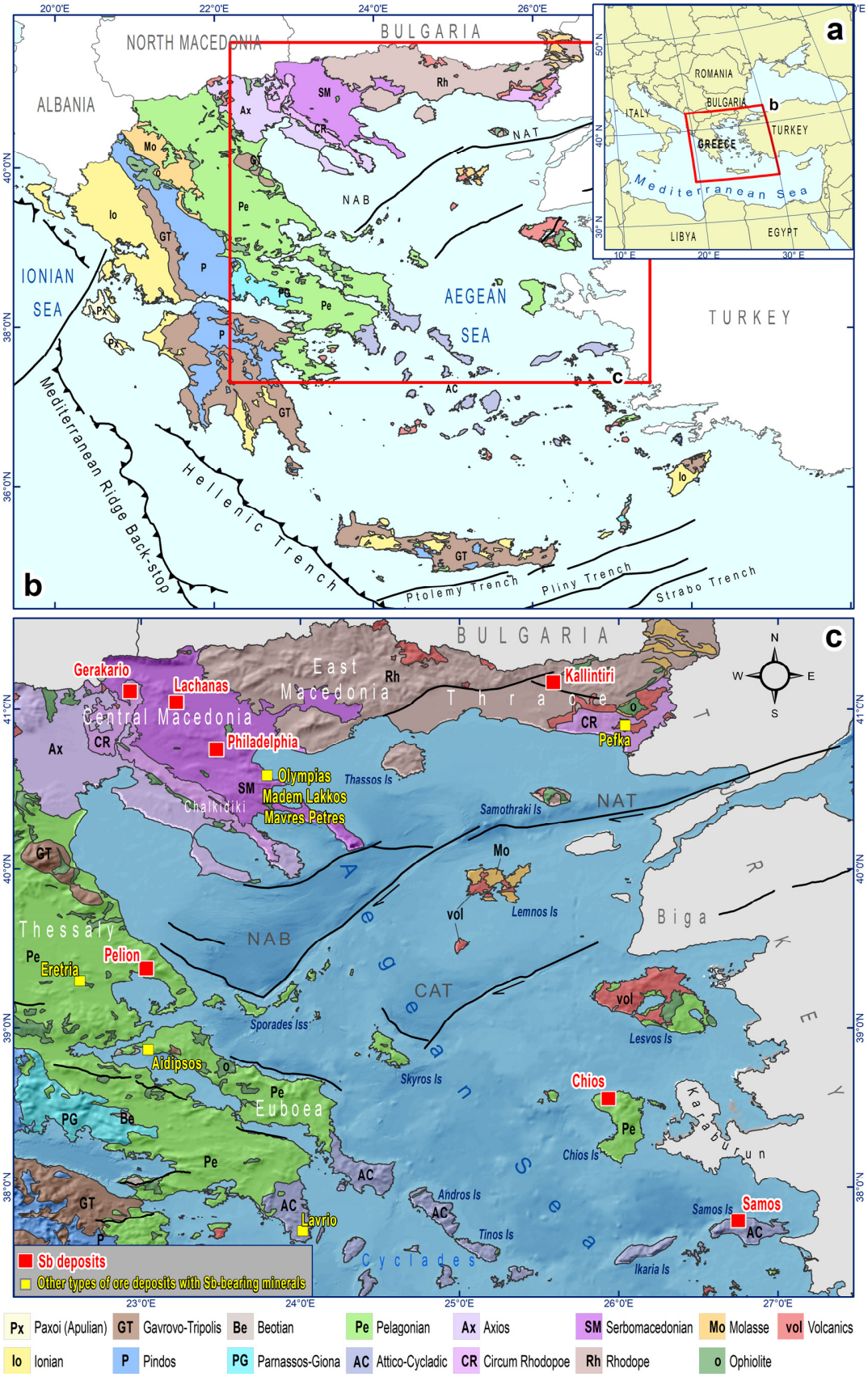

Figure 4. (**a**) The position of Greece in the East Mediterranean region. The red frame shows the location of map (**b**). (**b**) Geotectonic zones of Greece. Red frame shows the location of the map (**c**).

(**c**) Map of the antimony (Sb) ore deposits (yellow squares) and locations of other types of ore deposits with Sb-bearing minerals (blue squares) and the geotectonic zones, in which they are found.

3.1. Central—Eastern Macedonia and Thrace: Geology, Tectonic Setting, and Antimony Deposits

All antimony deposits in central Macedonia are located in the Serbomacedonian and Rhodope massifs of the Hellenic hinterland. Kilias et al. [63,77] distinguished five deformational events in Thrace since the Eocene: (i) event D1 lasted from the middle-late Eocene until the Oligocene; it is related to ductile tectonics and the formation of detachment faults, which resulted in the exhumation of the metamorphic core complexes (see also [45,76,78–80]; (ii) event D2 lasted from the late Oligocene until the early Miocene; it was related to transpressional tectonics under brittle conditions, which formed conjugate strike-slip faults (sinistral along NNE-SSW to NNW-SSE striking faults, and dextral along WNW-ESE to NW-SE striking faults), as well as thrust faults and folds with N–NW or S–SE sense of movement (see also [81]); (iii) event D3 lasted from the middle of the Miocene until the Pliocene; it was related to extensional brittle tectonics, which created large WNW-ESE to NNW-SSE oriented, high-angle normal to oblique-normal faults and reactivated some previous D2 structures under oblique motion (see also [76]); (iv) event D4 occurred in the Pliocene; it was related to the formation of large WNW-ESE to NE-SW striking, usually oblique-normal fault zones, which generally cut at a high angle the detachment fault of the D1 deformational event (see also [66,82]); and (v) event D5 is the most contemporary deformation event since the Pleistocene, related to the NNE-SSW oriented (σ_3 axis) extensional stress field and the roughly E-W striking and active normal faulting. In central Macedonia and the North Aegean Sea, three extensional tectonic phases are distinguished [66]: (i) a late Miocene, associated with a WNW-ESE-oriented σ_3-axis, (ii) a Pliocene—early Pleistocene, associated with a NE-SW- oriented σ_3-axis (see also [83]), and (iii) a mid-Pleistocene—Present day, associated with a N-S- oriented σ_3-axis. Concerning the NE-SW to ENE-WSW oriented faulting observed in the Greek Serbomacedonian massif, dextral to normal-dextral striations were measured [65,67], which are compatible with the Pliocene—early Pleistocene NE-SW extension. Plutonism in Rhodope spans between 55 and 21 Ma (Table 7 in [76] and references therein) and was related to early mid Cenozoic subduction and subsequent extension [80,84,85].

3.1.1. Kallintiri

In Kallintiri, exploitation of Sb ore took place during World War II under the control of German occupying troops. There is no known data regarding the amount of ore extracted.

According to Kanellopoulos et al. [86] and Kanellopoulos' unpublished data, the Kallintiri deposit represents a Sb-Pb-Zn-Ag-Au-Te mineralization, controlled by a structural trap in the brittle—ductile transition zone, but also found under brittle conditions. The main rocks in the area are late Eocene to early Oligocene porphyritic andesite with a fine-grained, granophyric groundmass dated by K-Ar geochronology at 30–31 Ma [72,75]. Additionally, late Eocene (?) volcano–sedimentary series affected by hydrothermal alteration crop out over extensive areas, accompanied by late Jurassic–early Cretaceous ophiolites mainly consisting of metabasalt, metagabro, and metadolerite, which belong to the Circum-Rhodope zone (Makri Unit; [75] and refs within). Two geothermal anomalies with hot springs are known in the south, including the Mitrikos Lake and Sappes geothermal fields. The ore body occurs within and above a low-angle normal fault, i.e., a detachment fault. The deposit is hosted by silicified marble and an argillic–sericitic altered schist in the Mesozoic Makri Unit and by marble, gneiss, and amphibolite in the Rhodope Massif, as well as within Eocene sandstone. It is present in the form of disseminations, high-angle quartz-barite–carbonate veins, and breccia. The stibnite mineralization is mainly hosted by vertical WNW-ESE- to NW-SE-oriented faults, which crosscut the detachment fault at high angles (Kanellopoulos, unpublished data; Figure 5) and could be associated with a late D1 to early D2 tectonics [63,77] implying an Oligocene deposition.

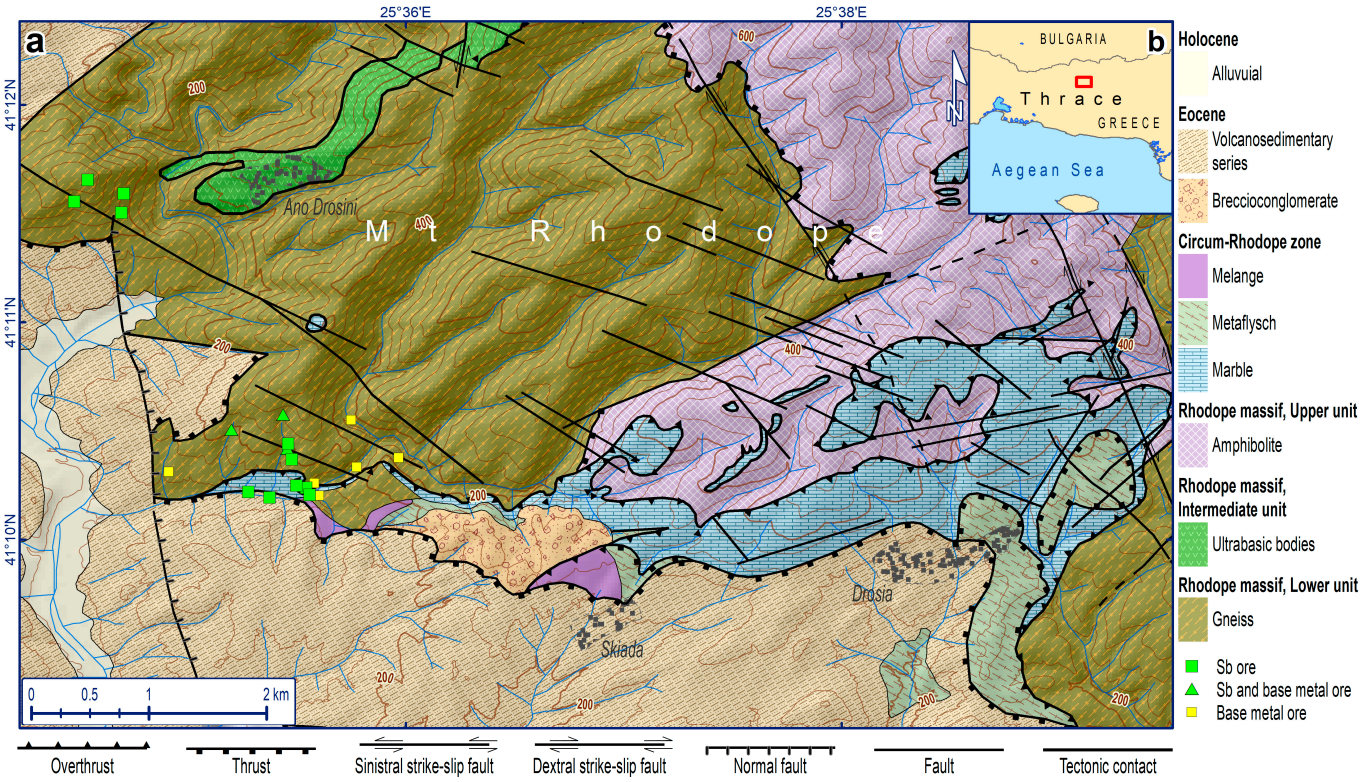

Figure 5. (**a**) Geological map of the Kallintiri area (modified after [37,86–88] and Kanellopoulos unpublished data). The Sb ore mineralization sites are shown with green boxes (based on [37,86,87] and Kanellopoulos unpublished data). (**a**) Inset map showing the location of map (**b**).

The process of ore deposition involved sequential precipitation, starting with the formation of pyrite including Au-Ag tellurides and native gold, followed by the development of iron-poor sphalerite, galena, chalcopyrite, bournonite, and minerals belonging to the fahlore group. It was followed by the deposition of Pb-Sb sulfosalts (semseiyte, zinkenite, fuloppite, senandorite, plagionite), and then by a Sb-As stage, characterized by the presence of antimonite, arsenopyrite, realgar and native antimony. The deposition of precious metals is in the form of electrum, gold–silver tellurides, and sulfosalts, namely Ag-rich tetrahedrite. The ore mineralization includes a Zn-Pb to Pb-Sb and Sb-As evolution [37,86].

The geochemical analysis conducted on the Sb-rich ore reveals an increased concentration of Hg, Te, and Tl inside the deposit [86] which is also supported by Kanellopoulos' unpublished data.

The Kallintiri deposit can be characterized as an intermediate to low-sulfidation epithermal mineralization. The presence of graphite intergrown with pyrite and galena in the Kallintiri mineralization is an unusual occurrence, indicating reducing fluids during ore deposition. Tellurides in the system provide evidence for a magmatic origin [86].

3.1.2. Lachanas

The Lachanas areas have a higher endowment of Sb-ore deposits than all other regions in Greece (Figure 6), including the Rizana and Lagkadas areas. Historically, several initiatives involving exploitation were conducted. Based on official records, it can be shown that mining was primarily targeting tungsten. It was initiated in 1915 and persisted throughout World War II under the control of German occupying troops. The first and predominant exploitation of Sb took place before 1930. Following World War II, in the 1950s, the region again saw the implementation of exploitation schemes. Between the 1930s and 1950s, underground mining activities resulted in the extraction of around 9000 metric tons of stibnite ore, with an average grade of 40% antimony [89].

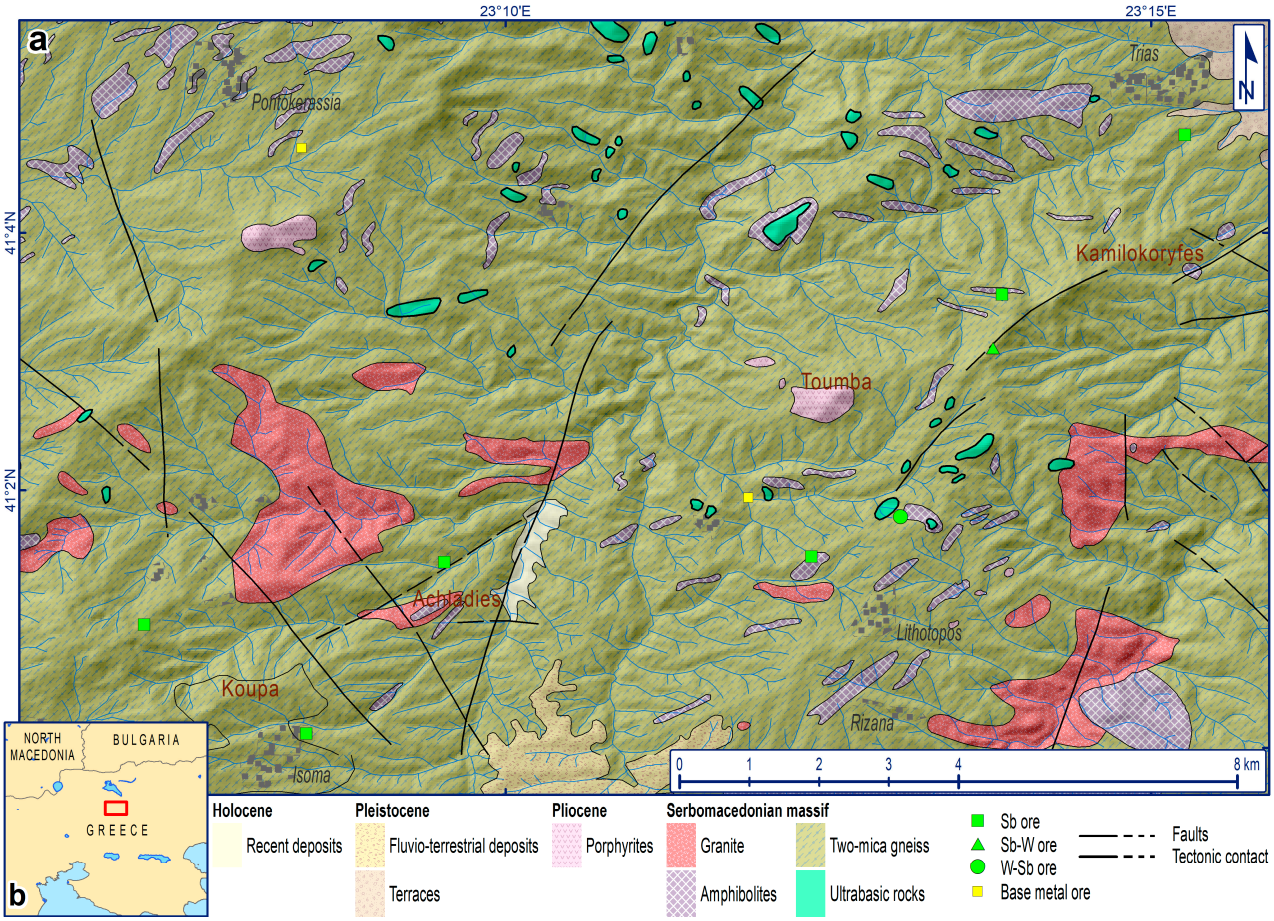

Figure 6. (**a**) Geological map of the Lachanas area (modified after [37,90–92]). The Sb and base metal ore mineralization sites are shown with green and yellow boxes, respectively (based on [37,89]). (**b**) Inset map showing the location of map (**a**).

An almost-pure Sb to Sb ± W-As ore body occurs in the area, whereas Zn-Pb sulfide minerals are absent [37]. Pliocene volcanic rocks, consisting mainly of rhyolite, dacite, and rhyodacite, are found in close proximity to the ore body in the area of Rizana and Lachanas ([75,90] and refs therein). These rock formations exhibit a porphyritic texture. Also, extensive hydrothermal alteration is present in the vicinity [90]. Older utrabasic rocks, i.e., peridotite–serpentinite from the Triassic age, which belong to the Serbo-Macedonia Massif (Vertiskos unit), can be found very close. Towards the NNE, a geothermal anomaly with hot springs can be found, i.e., the Lithotopos geothermal field (near Kerkini lake). Antimony mineralization at Rizana occurs in an NE-SW-oriented brittle shear zone intersecting a two-mica augen gneiss in the Vertiskos Unit. The ore bodies occur in the form of veins and discordant lodes, displaying massive and breccia textures. The hostrocks are affected by a halo of sericitization and silicification around the shear zone. The Rizana rhyodacite, exhibits sericitic alteration, includes disseminated pyrite, and appears to be associated with Sb-mineralization.

Stergiou et al. [89] reported that the mineralization in the Rizana region was formed within a restricted range of temperatures and salinities, as shown by fluid inclusion microthermometry. The fluid inclusions have low to slightly moderate salinities (6.6–8.1 wt% equiv. NaCl) with low homogenization temperatures (217–254 °C, with a maximum of 220 °C).

Ore deposition took place in two stages. In the first stage, fluids enriched with tungsten precipitated minerals such as wolframite, pyrite, and arsenopyrite. Subsequently, during the second phase, fluids enriched in antimony mostly deposited stibnite, along with minor

occurrences of chalcopyrite and gold. The primary occurrence of the ore is predominantly hosted by gneiss, namely white gneiss, and locally by micaschist and ultramafic rocks, such as listvenite. Highly silicified zones are closely associated with the ore bodies. In several cases, the ore is found within breccia, which occurs within a network of parallel faults within the region.

In the eastern part of this area, the Sb deposits seem to follow ENE-WSW- to NE-SW-oriented faults (Figure 6). If we also consider the tectonically controlled antimony mineralization at Rizana and the synchronous volcanism in this area, a deposition during the Pliocene–early Pleistocene can be inferred.

The mineral composition of the ore assemblage includes stibnite, berthierite, sphalerite, pyrite, chalcopyrite, native antimony, as well as trace amounts of wolframite, arsenopyrite, galena, marcasite, pyrrhotite, realgar, tetrahedrite, boulangerite, native arsenic, and native gold. Additionally, quartz, along with minor quantities of ankerite and barite, are present as gangue minerals. Valentinite, goethite, and claudetite are among the minerals associated with oxidation [37,89,93]. Dimou et al. [37] have identified traces of As (up to 0.550 wt%), Pb (up to 0.311 wt%), Sn (up to 0.532 wt%), and Fe (up to 0.016 wt%) in the stibnite, while Tzamos et al. [93] identified significant amounts of Hg (up to 10.08 ppm) in stibnite.

The analysis of bulk ore geochemistry reveals enrichments in some elements, including As, Au, Cd, Se, Tl, and W [89].

3.1.3. Gerakario

A Cu-Au porphyry deposit occurs in Gerakario and epithermal quartz–stibnite veins are also located in the eastern part of the deposit, crosscutting the two-mica gneiss (Figure 7). In the vicinity of the Cu-Au, Cu, and Sb mineralization in the Gerakario and Divouni region, Pliocene subvolcanic rocks occur, similar to the Rizana area. They are predominantly composed of rhyolite and dacite [75,90] and refs within. These rock formations exhibit a porphyritic texture. Mineralization occurs in the form of stockworks, veins, and breccia, with silicification, sericitization, propylitization, and chloritization being the most common types of alteration present in the area [90]. Older peridotite–serpentinite from the Triassic age, which belongs to the Serbo-Macedonia Massif (Vertiskos unit), are found nearby. According to Stergiou et al. [94] the A-type veins found in the porphyry-style mineralization exhibit fluid inclusions that indicate fluid boiling. This process led to the formation of a highly saline aqueous fluid phase (with a concentration of 35.7 to 45.6 wt.% NaCl equivalent) and a moderately saline gas phase (with a concentration of 14 to 22 wt.% NaCl equivalent) within the H_2O-NaCl-KCl system. These fluid inclusions are observed at temperatures ranging from 380 to 460 °C and pressures ranging from 100 to 580 bar. Mixing of moderately saline fluid and meteoric water resulted in the formation of lower salinity fluids (containing 8 to 10 wt.% NaCl equiv.), which are linked to the formation of epithermal quartz–stibnite vein mineralization. The aforementioned process occurred within a range of hydrostatic pressures spanning from 65 to 116 bar, at a depth ranging from 600 to 1000 m. The prevailing temperatures were mainly within the range of 280 to 320 °C.

The Sb-mineralization mostly comprises arsenopyrite, pyrite, berthierite, stibnite, native antimony, and pyrrhotite, with small occurrences of marcasite, chalcopyrite, löllingite, and native gold [94,95]. The occurrence of native Sb indicates that the fluids were supersaturated with respect to antimony. The examination of stibnite using laser ablation inductively coupled plasma mass spectrometry (LA-ICP-MS) reveals elevated concentrations of base metals, including Cu and Pb. Additionally, stibnite exhibited relatively notable concentrations to several elements, such as Ag, As, Bi, Ce, Co, Fe, La, Re, Sm, Th, Ti, and Tl [94,95].

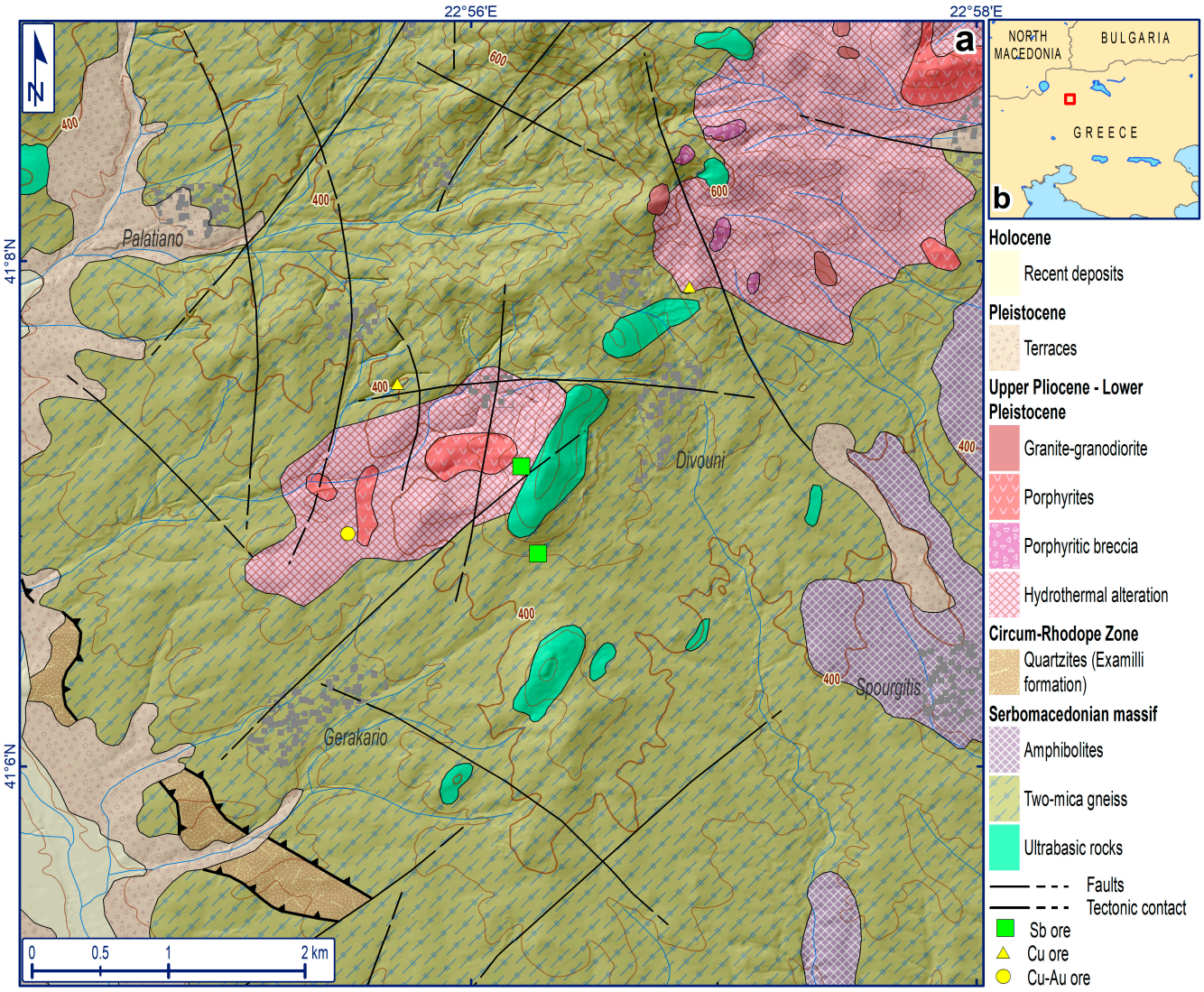

Figure 7. (**a**) Geological map of the Gerakario area (modified after [93]). The Sb and other types of ore sites are shown with green and yellow boxes, respectively (based on [94,95]). (**b**) Inset map showing the location of the map (**a**).

Bulk geochemical analyses demonstrate a notable concentration of critical and rare metals, such as Ag, Au, Bi, Ce, Co, Ga, La, and Sb [94].

As in Lachanas, the Sb mineralization in this area is also tectonically controlled [94,95], which is expected given that both sites are close. Thus, the same deposition age (Pliocene–early Pleistocene) can be inferred.

3.1.4. Philadelphia

In the Philadelphia area, the Sb mineralization was known before World War II, and a small-scale exploitation by a private company occurred then.

The Sb mineralization in Philadelphia occurs in metamorphic rocks (Figure 8), including amphibolite and gneiss. In the greater area, around the mineralization, extensive geothermal anomalies and hot springs are found, i.e., to the NW are the Nimfopetra and Nea Apollonia geothermal fields (south of Volvi lake), and SE the Therma Nigritas geothermal field. In contrast to Lachanas and Gerakario, recent volcanic rock occurrences are lacking in this area. Instead, only Triassic granite intrusions (231.6 ± 9.9 Ma, [96]), as well as Triassic ultramafic rocks, are present, although the mineralization occurs in the same geotectonic unit (Serbo-Macedonian massif, Vertiskos unit). According to Dimou et al. [37],

this mineralization is controlled by mainly N-S-oriented, E-dipping, and NE-SW-oriented, SE-dipping fault-systems with an average 60° dip angle. Locally, these fault systems consist of a dense fault network of a few major and many secondary diffused fractures that cannot be displayed on medium-scale maps. This fault system can be attributed to the Pliocene–early Pleistocene tectonic phase, implying that the antimony is syntectonic.

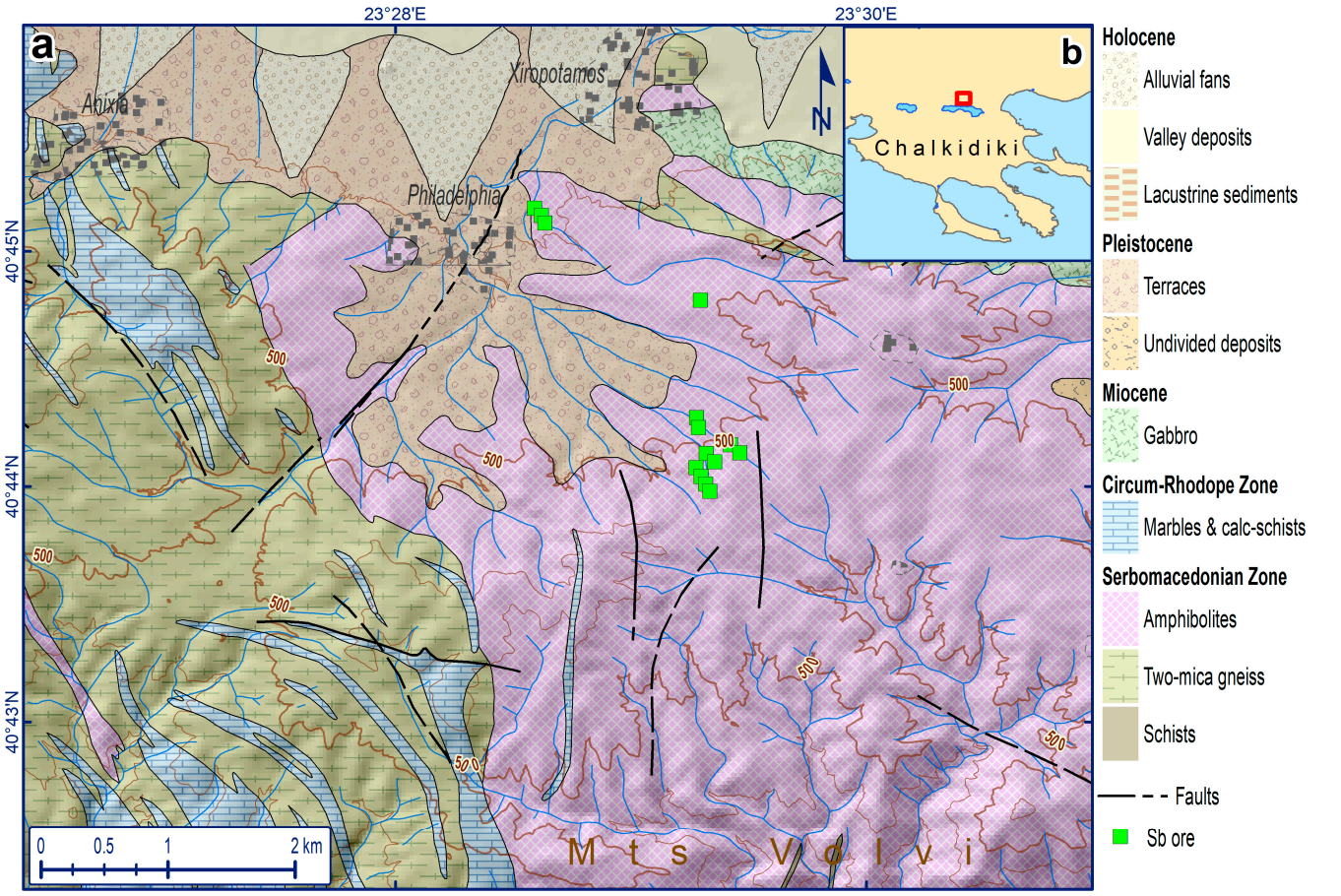

Figure 8. (**a**) Geological map of the broader Philadelphia area (modified after [97,98]). The Sb ore mineralization sites are shown with green boxes (based on [37]). (**b**) Inset map showing the location of map (**a**).

The faults have an up to 1 m wide opening and are filled with mineralization due to the infiltration of silicic fluids. Mineralization is characterized by the presence of a quartz gangue, accompanied by the hydrothermal alteration (i.e., sericitization) of the surrounding rock formations. The mineralization includes an early stage with restricted occurrence of base and precious metals, such as sphalerite, pyrite, arsenopyrite, and gold, whereas antimony ore, including stibnite, chalcostibite, tetrahedrite, zinkenite, and kermesite, prevails in the second stage. The presence of galena and Pb-Sb mineral phases is lacking [37]. Dimou [37] has identified traces of As (up to 0.524 wt%) and Sn (up to 0.594 wt%) in the stibnite.

3.2. Chios Island Geology, Tectonic Setting, and Antimony Deposits

Chios Island is dominated by late-Palaeozoic to Mesozoic, very-low-grade metamorphic sequences of the Pelagonian zone [99,100]; the origin of which varies as several models have been proposed, such as the occurrence of a subduction/accretionary complex, a mid-ocean ridge, or a rift (e.g., [101–106]). Especially on the northwestern part of the island, where the antimony deposits are found, lithology consists of Palaeozoic–early Triassic clastic rocks (greywacke) bearing olistoliths and intercalations of older age and various

compositions (volcanic rocks, limestone, volcanic and quartz tuff), characterized as 'Chios mélange', 'Chios (wild) flysch', or 'Volissos turbidites' [101,104,107], representing the basal formation of the Lower ("autochthonous") Unit [99,108–111]. Additionally, volcanic rocks, i.e., rhyolite, are found close to the base metal and Sb mineralization in Agioi Pantes-Kambi. According to Pe-Piper et al. [110], the rhyolite contains phenocrysts composed of sanidine, quartz, plagioclase, and biotite. The groundmass of the rhyolite is microcrystalline and contains flow lamination. The age of the rhyolite was determined as middle Miocene (14.7 ± 0.7 by K-Ar dating, [111]).

From the post-Alpine tectonics of Chios, only the recent-active stress field regime is known [112]. However, the ductile extension that produced the detachment faults in Thrace and Samos [49,63,113], which is associated with the Hellenic Subduction's back-arc extension and its southward migration, must have passed through the island. In any case, detachment faults do not crop out on the island in contrast to the opposite Turkish side to the east (Menderes metamorphic core complex; e.g., [114–117]). The active tectonics on Chios Island are quite complex: although the prominent active faulting is normal with an E-W direction, faults occur in other directions with either normal or oblique-normal movement [115] many of which are probably older faults reactivated under the present stress field regime. It is noteworthy that directly to the east of Chios, along the central–western Turkish coast, N-S- to NE-SW striking, dextral strike-slip faults cross the Karaburun peninsula and the Izmir Gulf (e.g., [118–120] proving that a shear co-existed with the N-S extension.

The antimony deposits are located on the northern part of the island, exclusively in the Palaeozoic clastic rocks, mostly along a roughly linear, N-S-oriented axis (Figure 9). This alignment coincides with two aligned, nearly linear river torrent valleys (Alvanos to the north and Halikias to the south), which flow in different directions (northward and southward, respectively) draining the north and south slope, respectively, of the Palaeozoic Amani Mt. This nearly linear morphological feature possibly has a tectonic origin that is similar to the N-S-oriented faults found in the Karaburun peninsula. The age of this tectonic structure is hard to pinpoint. If we also consider the occurrence of hot springs in the valley's estuary (Ayasmata) and the N-S-oriented faults in the Karaburun peninsula (Turkey), then this tectonic structure could be interpreted as being active recently; however, its initial formation might be even older, as old as the nearby middle Miocene volcanic rocks. Several exploitation projects took place during the 1910's, 1940's and 1950's, by private companies aiming for the Sb ore.

In the past, the prevailing view was that mineralization was stratabound within the late Paleozoic sediment rocks; however, our current understanding suggests that it was controlled by tectonic processes. Specifically, the mineralization is hosted by faults that crosscut the stratification of clastic sedimentary rocks or the replacement of Silurian carbonate [121,122]. It is notable that the excavations are situated close to geological faults.

Hydrothermal alteration is observed in the clastic sedimentary wallrocks, i.e., quartz–sericite–pyrite assemblage, whereas ankeritization is observed in the carbonate rocks.

The mineralization is classified as hydrothermal with a low Au concentration [122]. This mineralization is associated with the intrusion of mid-Miocene porphyritic rhyolite into the autochthonous unit (Agioi Pantes and Kambia). Skarpelis [122] suggests a potential correlation between the mineralization in Chios and the Miocene epithermal hydrothermal deposits found in Western Turkey.

This particular site in Greece represents the only occurrence where the main Sb minerals are stibnite and berthierite [121]. It is important to note that the system under consideration lacks the presence of As, making it the predominant Sb ore with a high Fe content in Greece. The primary mineral phases identified include stibnite, berthierite, melnicovite, with pyrite (both typical and framboidal forms), chalcopyrite, sphalerite, arsenopyrite, graphite, and valentinite occurring as secondary mineral phases. Skarpelis [122] also found tetrahedrite as an additional mineral.

The primary deposit has modest Au and Ag grades. According to Dimou et al. [121] and Skarpelis [122], the mineral composition of the ore assemblage includes stibnite (two types according to Dimou et al. [121]), berthierite, melnicovite, pyrite (both typical and framboidal forms), chalcopyrite, arsenopyrite, graphitoide, sericite, and valentinite. Dimou et al. [121] have identified traces of As (up to 0.554 wt%), Pb (up to 0.608 wt%), Bi (up to 1.538 wt%), Sn (up to 0.009 wt%), Cu (up to 0.016 wt%), Zn (up to 0.035 wt%), and Fe (up to 0.758 wt%) in the stibnite.

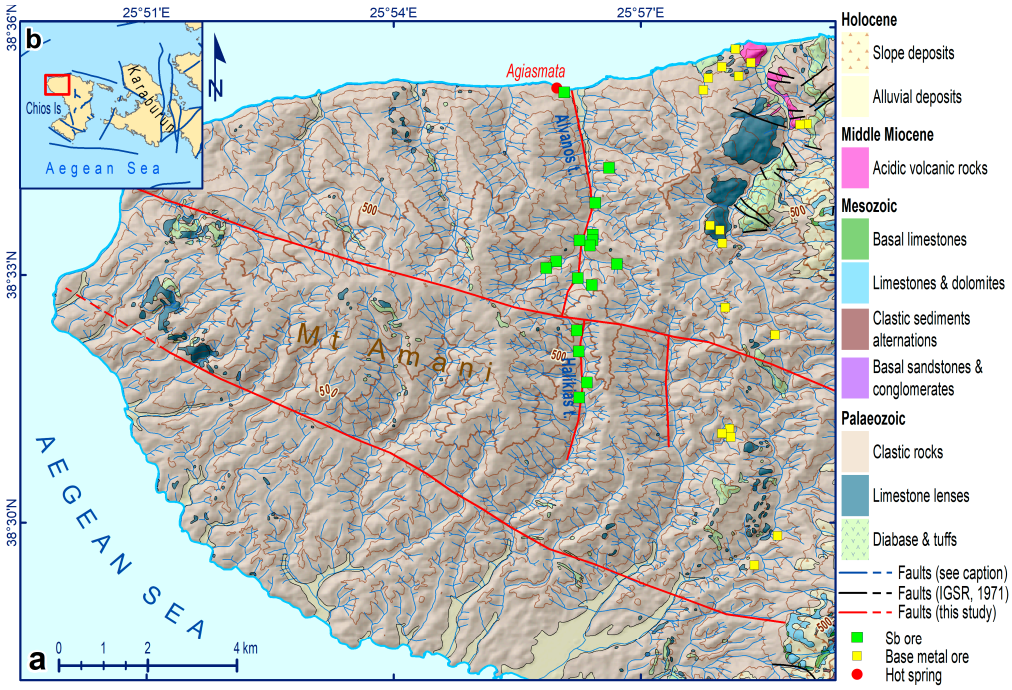

Figure 9. (**a**) Geological map of the NW part of Chios Island (modified after [123]) and the main active faults after the synthesis of [112,118–120]. The Sb and base metal ore mineralization sites are shown with green and yellow boxes, respectively (based on [121]). (**b**) Inset map showing the location of the geological map (**b**).

3.3. Samos Island Geology, Tectonic Setting, and Antimony Deposits

The Alpine bedrock of Samos Island consists of a pile of nappes belonging to three tectonostratigraphic units (from lower to upper; [115,123–125]: (i) the Basal Unit (metamorphic equivalent of the Gavrovo-Tripolis zone); (ii) the high-pressure metamorphic Cycladic Blueschist Unit; and (iii) the Upper Cycladic Nappe. During the (late) Miocene extension, detachment faults (e.g., the Kallithea detachment fault at the western part of the island) revealed the Basal under the Upper Cycladic Nappe [113,115,125]. Additionally, volcanic rocks, i.e., mainly trachyte and in some cases rhyolite, as well as pyroclastic material and silicified sedimentary rocks, are found close to the base metal and Sb mineralization. Pe-Piper et al. [126] assert that the emplacement of the trachyte occurred in the context of regional extension and listric faulting. Subsequently, the emergence of N-S-oriented strike-slip faults facilitated the extrusion of basalt and rhyolite with ages ranging from 8.0 to 8.5 Ma. The age of the trachyte was determined as being late Miocene (10.2 ± 0.3 Ma by K-Ar dating, [75]).

Ring et al. [118] have recognized five deformational events on the island of Samos: (i) events D′1 and D′2 lasted from the Eocene to the early Oligocene; they were related to crustal contraction and to the blueschist and blueschist–greenschist facies metamorphism, and they are responsible for the nappe-stacking; (ii) event D′3 lasted from the early Oligocene until the middle–late Miocene; it was associated with crustal extension under ductile to brittle conditions and, hence, detachment faulting; (iii) event D′4 lasted for a

short period in Tortonian (late Miocene); it was associated with the late stage extension parallel folding and the development of E- and W-dipping faulting; and (iv) event D'5 is the contemporary deformational stage since the late Miocene; it is related to brittle extension, which has formed E-W- to NW-SE-oriented normal faults (see also [112,127,128]. As already mentioned above, the intrusion of the igneous rocks (monzodiorite, granite, trachyte, basalt, and rhyolite) on Samos Island can be associated with large-scale extension parallel folding of the detachment and the development of faults along the margins of the supradetachment basins [74].

In Samos Island, exploitation activity has been known in the greater area since 1880, in which the main target was base metal mineralization, but Sb mineralization and gold were also extracted.

The Sb mineralization is situated in the eastern margin of the Karlovasi basin (North-central part of the island), controlled by a NNE-SSW- to NE-SW-striking, W-dipping conjugate fault system that intersects the silicified conglomerate (Figure 10) [100]. Similar to the Kallintiri (Thrace) case, the main mineralization was associated with the intrusion of the volcanic rocks and the synchronous D'3 deformational phase with the ductile detachment faulting facilitating the hydrothermal fluid circulation and the Sb deposition; these processes were further continued in the following D'4 deformation event. Accordingly, the Sb deposition should have occurred in the late Miocene to early Pliocene age. It is a hydrothermal, epithermal-type mineralization, tectonically controlled, and genetically related to the late Miocene volcanism. The first arrival of Si-rich fluids preceded the subsequent silicification of the rock formations. Following this, fluids with reduced Si content deposited stibnite and pyrite. Finally, in the final stage, the deposition of melnicovite, fluorite, and barite took place. As and Pb are almost nonexistent in the mineralization.

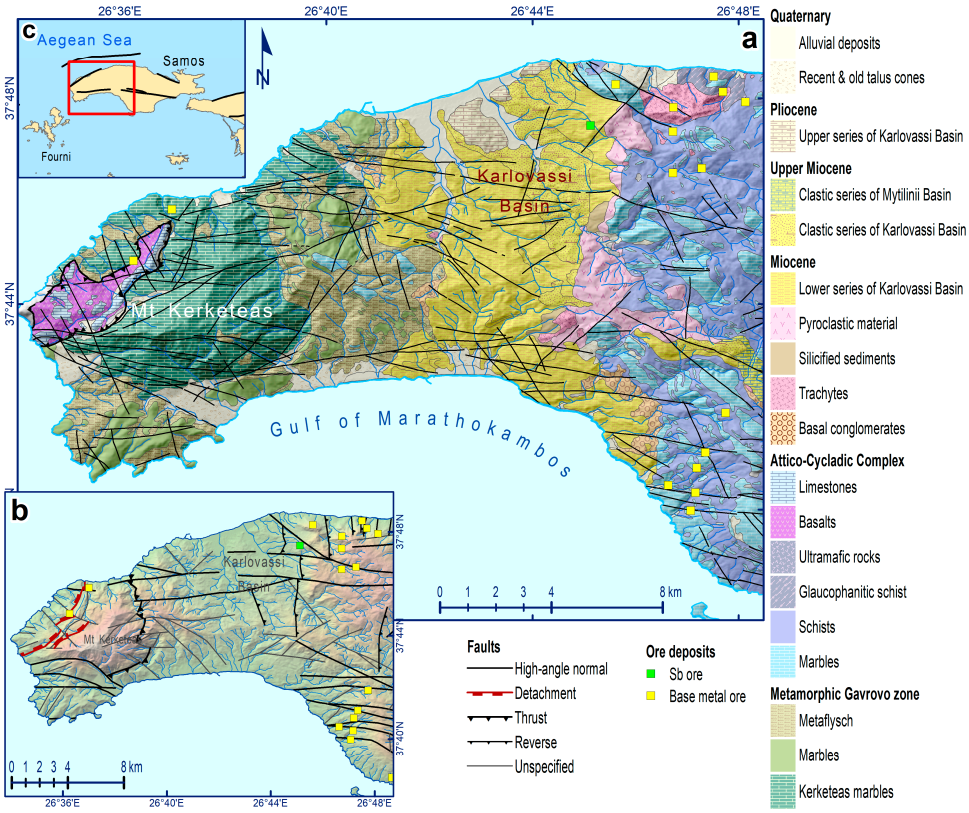

Figure 10. (**a**) Geological map of western Samos Island (modified after [123]). The Sb and base metal ore mineralization sites are shown with green and yellow boxes, respectively (based on [95]). (**b**) Tectonic map of western Samos Island (after [113]). Faults legend is common for (**a**,**b**). (**c**) Inset map of the broader area showing the location of maps (**a**,**b**) (red rectangular) and the active faults (after [112]).

According to Dimou et al. [95], stibnite is the primary ore mineral and the mineral composition of the ore assemblage includes stibnite, pyrite, melnicovite, quartz, fluorite, and barite, while Pb-Sb sulfides are totally absent, similar to previously mentioned systems, i.e., Philadelphia. The mineralization is located in the silicified conglomerate, as cement or inside fluorite geode assemblages. Dimou et al. [95] have identified traces of Fe (up to 0.033 wt%), Cu (up to 0.016 wt%), Ag (up to 0.017 wt%), Pb (up to 0.206 wt%), Bi (up to 0.183 wt%), and As (up to 0.435 wt%) in stibnite.

3.4. Pelion (SE Thessaly) Geology, Tectonic Setting, and Antimony Deposits

Southeast Thessaly is situated in the broader Pelagonian zone. In the Pelion region, the antimony hosting formations are Permian–early Jurassic ortho- and para-metamorphic rocks consisting of schist, schist–gneiss, quartzite, and phyllite, intercalated by marble [129]. Additionally, volcanic rocks, i.e., mainly diorite or diabase dykes, occur in the area. According to Tataris [130] the diorite exhibits a holocrystalline granitoid porphyritic texture. The age of the volcanic rocks was determined to be Pliocene (5.2 ± 0.7 to 3.9 ± 0.2 Ma by Ar/Ar dating; [131]). The Late Cenozoic tectonic history of Thessaly has been described by Caputo and Pavlides [62] who documented three phases: (i) a late-orogenic compressional phase (roughly E-W oriented σ_1 axis) during the early middle Miocene period, which reactivated the older NW-SE-oriented Alpine thrusts; (ii) a Pliocene—early Pleistocene extensional phase (ca. NE-SW oriented σ_3 axis, as in the northern mainland Greece and Aegean Sea), which formed most of the marginal NW-SE-striking normal faults quasi-parallel to the older thrusts; and (iii) a middle Pleistocene–present extensional phase (ca. N-S oriented σ_3 axis) which formed the roughly E-W-striking normal faults whose morphological expression overprints the NW-SE structures.

Tataris [130] states that antimony mineralization in the Pelion area was known since the very late 19th century.

The presence of antimony in Pelion is characterized by early Sb-Zn and late Sb-As ore assemblages. The first deposition consisted of pyrite, sphalerite, and arsenopyrite, followed by the subsequent deposition of the early stage stibnite. Finally, both late-stage stibnite and realgar were deposited [121]. The early stage mineralization is hosted by cipoline-marble horizons that are present in schist formations. Furthermore, it is seen that stibnite that has undergone recrystallization is found inside quartz veins that intersect the schist [121]. This observation suggests that the formation of stibnite is hydrothermal and influenced by the local tectonic activity, probably the middle Pleistocene–Present day one.

Pelion mineralization is a monometallic to two-metallic one, with a main ore, the Sb, which seems to be tectonically controlled. Pliocene volcanic rocks occur in the greater area, and Pb is absent.

As seen in the maps in Figure 11, the base metal ore mineralization follows lineaments in both the ENE-WSW- and NW-SE-oriented neotectonic (recent) fault systems (map (b) of Figure 11; [132]), especially in the eastern part of the peninsula, toward the Aegean Sea. Although the NW-SE-striking faults could be associated with previous tectonic phases (e.g., the Pliocene–early Pleistocene one), these particular ones, along the eastern coast of the Pelion peninsula (Aegean Sea), are considered marginal active faults of the NAB (Figure 11c; [132]). Towards the western part of the peninsula, near the Pagasitikos Gulf coast, the Sb ore site seems to be located next to two faults which have been recognized in this study from high-resolution satellite images cutting and displacing the Mesozoic marble of the Pelagonian zone. These two faults follow the same direction as the Pliocene–early Pleistocene faults of this area. In any case, the Sb deposition along the fault systems should have occurred during the Pliocene.

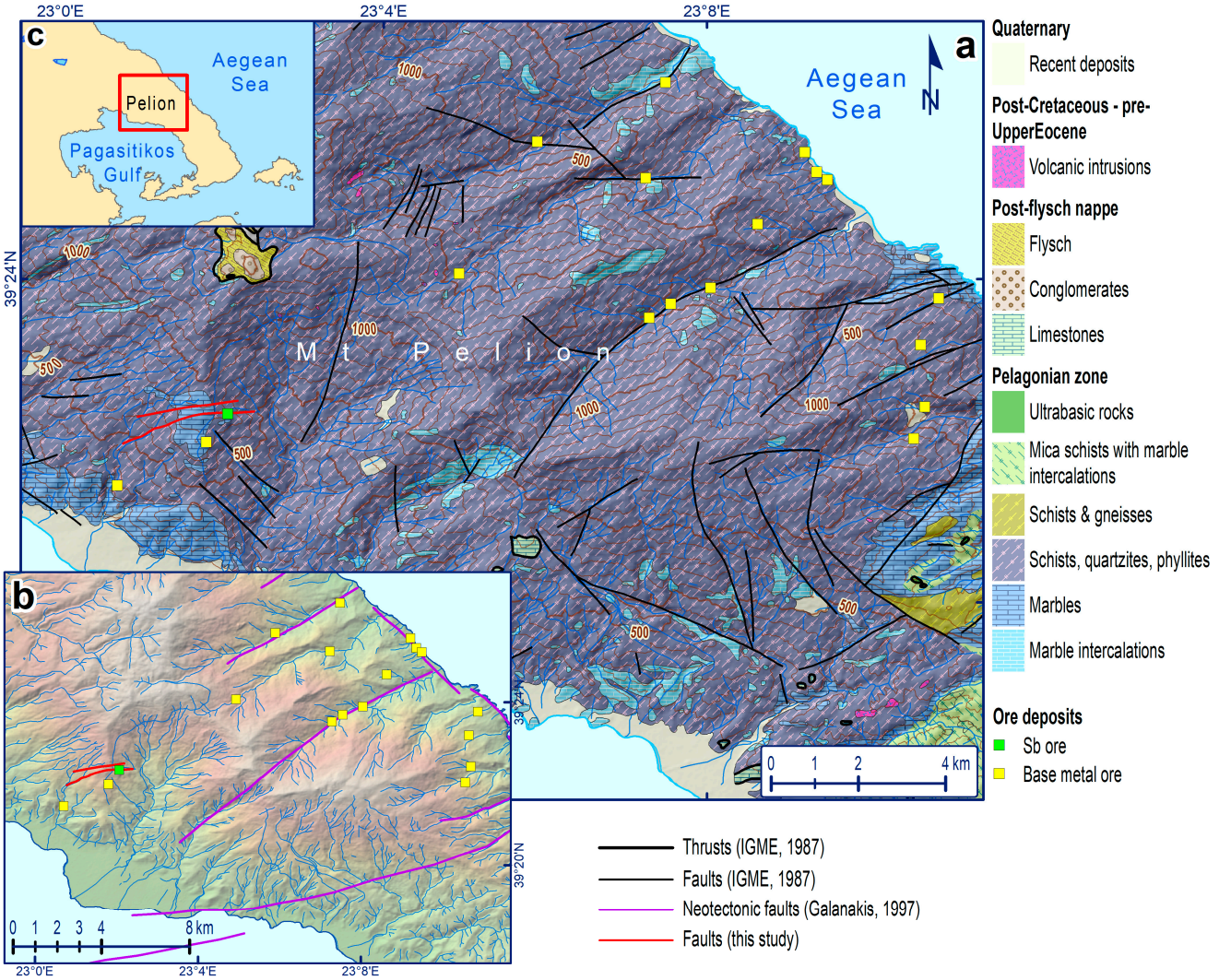

Figure 11. (**a**) Geological map of Pelion area modified according to [129]. The Sb- and base-metal-ore mineralization sites are shown with green and yellow boxes, respectively (based on [121,130]. (**b**) Shaded relief map showing the neotectonic faults in purple colour by Galanakis [132] and the faults detected from satellite imagery in this study in red colour. (**c**) Inset map showing the location of (**a**,**b**).

According to Dimou et al. [121] the ore assemblage includes stibnite, pyrite, sphalerite, arsenopyrite, tennantite and realgar. Dimou et al. [121] have identified traces of As (up to 0.454 wt%), Bi (up to 1.492 wt%), Pb (up to 0.449 wt%), Zn (up to 0.036 wt%), Cu (up to 0.021 wt%), and Fe (up to 0.031 wt%) in the stibnite.

3.5. Minor Occurrences of Antimony in Other Type of Deposits

Antimony mineral phases have been identified in some cases as being minor mineral components in complex polymetallic deposits, usually related to base metal mineralization, but also in active geothermal mineralizing systems. Most of these cases are located in the Greek Rhodope, where most of the Sb deposits are also located (Figure 4).

One of these cases is the Pefka area, where a Cu-Au-Te-In-Se polymetallic ore deposits occur [133–136]. The Pefka area is characterized by epithermal-style alterations and mineralization hosted by andesitic lavas. Two distinct styles of mineralization occur at the Pefka resource: (1) early NNW-oriented, high-sulfidation (HS) quartz, enargite/luzonite, and gold veins; and (2) later NE-oriented, intermediate sulfidation carbonate veins and breccia-hosting tennantite and tellurides, which locally overprint the HS veins. The enargite-Au

and the carbonate-telluride veins are enveloped by the host rock's sericitic to argillic and intermediate argillic alteration, respectively. Sericite and barite are gangue minerals in the enargite-bearing veins. Stibnite has been reported as a minor mineral and is associated with tellurantimony and chalcostibite during the telluride stage [136]. Stibnite has traces of Fe (up to 0.070 wt%), Cu (up to 0.079 wt%), Pb (up to 0.237 wt%), Bi (up to 0.041 wt%), and As (up to 0.448 wt%) [100].

The NE part of the Chalkidiki peninsula (the Kassandra mining district) contains one of the largest polymetallic Au-Ag-Pb-Zn-Cu carbonate-hosted replacement orebodies in Europe (i.e., at Olympias, Madem Lakkos, and Mavres Petres), hosted in marble and gneiss in the Rhodope Massif [137,138]. Various plutonic to subvolcanic intrusives were emplaced in the district during the Cenozoic period. The carbonate-hosted replacement massive sulfide orebody at Olympias contains a complex sulfide mineral assemblage ranging from coarse-grained galena-sphalerite dominant to pyrite-rich massive sulfide containing arsenopyrite and chalcopyrite [137,138]. Boulangerite-bearing siliceous breccia appears transitional with arsenopyrite-rich sulfide zones. The carbonate-hosted replacement deposit at Stratoni consists of the Madem Lakkos and Mavres Petres orebodies. Both orebodies exhibit galena-sphalerite +/− pyrite and a variety of sulfosalt minerals, such as boulangerite [137,138]. In the Stratoni deposit, stibnite enriched in Se (10 ppm) and Ag (27 ppm) associated with boulangerite has been reported [93]. Additionally, in Olympiada stibnite, accompanying bournonite and boulangerite, is enriched in As (up to 157 ppm), Sn (up to 83 ppm), Ag (up to 70 ppm), and Tl (up to 15 ppm). Bournonite and boulangerite are enriched in Bi (up to 1610 ppm), Ag (over 200 ppm), Tl (up to 92 ppm), Cd (up to 22 ppm), and Sn (up to 70 ppm) [93].

A polymetallic ore mineralization consisting of mixed sulfide ore minerals, which also has Mn-ore mineralization with alabandite and Mn-rich sphalerite, was found at Stagira. Stibnite occurs as a minor mineral phase and has traces of Fe (up to 0.033 wt%), Cu (up to 0.016 wt%), Ag (up to 0.017 wt%), Pb (up to 0.206 wt%), Bi (up to 0.183 wt%), and As (up to 0.435 wt%) [95].

The Laurion district includes several Pb-Zn-Cu-Ag-Au polymetallic carbonate-replacement, vein- and breccia-style orebodies hosted mainly in marble and a schist of the Attico-Cycladic massif [139–142]. Galena-bearing ores were exploited for silver and lead during the ancient times and the recent past [143]. The primary minerals associated with antimony ore include bournonite and tetrahedrite [139,140,144]. The presence of Sb-bearing minerals from the oxidation zone was also detected in the Kamariza region by Solomos et al. [145]. The antimony-enriched association includes minerals such as stibiconite, bindheimite, mimetite, and gartrellite. A major Pb-As-Sb-Cu-Ag rich banded vein, known as "Vein 80" or "Filoni 80", in the Plaka area contains various Sb-bearing sulfosalts and stibnite [139,146]. Antimony bearing minerals at vein 80 include among others pyrargyrite, miargyrite, stephanite, tetrahedrite, bournonite, lead sulphantimonides such as heteromorphite, semseyite, and veenite [139].

In the Eretria area (Thessaly), close to Pelion, the hosting formations are ultrabasic rocks consisting of serpentinite, peridotite and dunite [147]. Near Eretria there are significant chromite ore exploitation sites, with sulfides [148]. In some of them, the mineralization of sulfides is less developed and is characterized by the absence of Cu and the presence of Sb and As. The ore mineral paragenesis consists of chromite, ferritchromite, magnetite, pentlandite, Ni-cobaltite, millerite, heazlewoodite, niccolite, breithauptite (NiSb), valleriite, marcasite, and orcelite [148]. The occurrence of an E-W-oriented neotectonic fault [149] may have contributed to the mineralization.

Finally, active ore-bearing thermogenic travertine in northwestern Euboea Island, mainly in the Aidipsos area and the neighboring part of the mainland in eastern Central Greece, i.e., Sperchios area, are the surface manifestations of an active hydrothermal system, controlled by active tectonics, and supplied with heat by a 7–8 km deep magma chamber, with surface manifestation, the Plio-Pleistocene trachyandesitic volcanic center

of Lichades [150,151]. Several metallic mineral phases including sulfides (such as pyrite, arsenopyrite, galena, chalcopyrite, sphalerite, and stibnite), native elements (such as Pb and Ni) and native iron [152], alloys (such as Au ± Cu-Ag), fluorite, and REE-bearing phases were identified as being syngenetically enclosed as clastic grains within the pores of all studied travertine [150]. The northwestern Euboea Island hydrothermal system represents the first documented active terrestrial mineralizing hydrothermal system associated with ore-bearing travertine in Greece [150,151,153].

4. Discussion and Conclusions

Antimony is recognized on a global scale as a critical raw material of significant importance, based on its uses in several sectors such as green energy, high technology, electronics, and particularly in the field of energy transition, mostly due to its role in large-capacity storage batteries.

One of the primary challenges nations encounter when they are reliant on consistent and secure access to a critical natural resource, such as antimony, to meet their industrial requirements is the inequitable global allocation and production of these resources. The identification of other resources of antimony may be a significant problem for countries heavily reliant on this element. Mainly China along with Russia and Tajikistan were and still are the dominant producers. However, since 2011, production of antimony in China has declined.

The heavy reliance of several antimony-consuming nations on a small number of antimony-producing countries raises apprehensions over the integrity of the supply chain and jeopardizes the prospects of sustainable development. Antimony deposits are seen in several geological formations, including diverse deposit types with varying ages. Notably, the concentrations of ore-grade antimony are often limited, and a modest size and discontinuity typically characterize the presence of pure stibnite deposits. The presence of many parameters makes exploring antimony deposits a complex challenge. Consequently, there is an urgent need to identify more antimony deposits and re-evaluate those currently known. Furthermore, it is crucial to establish a societal consensus among the local population in any endeavor involving antimony exploitation projects in Western nations.

Greece is a member of the EU and has many antimony deposits. In some of these deposits, exploitation projects took place, particularly in the early 20th century and during World War II, by occupying troops. Unfortunately, no records exist about the quantity of ore mined during this period. Some deposits contain antimony as the primary commodity, specifically stibnite deposits like Lachanas and Philadelphia. Additionally, there are deposits in which antimony is one of several primary commodities. In these cases, antimony can be obtained along with the other commodities, such as in the Kallintiri deposit. Furthermore, the occurrence of Sb minerals in other types of mineralization is scarce, rendering them unsuitable as a target for exploratory endeavors due to their limited presence (i.e., Lavrio, Pefka, Eretria–Thessaly).

The majority of antimony deposits exhibit characteristics of hydrothermal origin, controlled by tectonic processes and associated with Cenozoic magmatism (Table 1). In some cases, these deposits present close geochemical affinities and generally demonstrate a transition to mixed-polymetallic deposits. Tectonic activity in combination with magmatic intrusions seems to have played a significant role in the antimony deposition, as faulting enhances permeability, facilitates upwards hydrothermal fluid circulation, and hence, the mineral deposit formation, especially when faulting was active (e.g., [154,155]). On-site observations (e.g., [37,86,95,121] and Kanellopoulos' unpublished data) suggest that Sb deposition took place in fault gauges and damage zones in most areas in this study. In Kallintiri (W. Thrace) and Samos Island (Aegean Sea), the intrusion-synchronous detachment faults in the back-arc southward migration of the extension are the protagonists of the Sb mineralization, which was facilitated even more by the following brittle deformational events; hence, a late-Oligocene and early Miocene-age Sb deposition can

be inferred for these two regions, respectively. Since Sb deposition in the eastern part of Greece is related to the back-arc extension's migration, the middle Miocene intrusions of Chios Island are in the migration's pathways before reaching Samos Island to the south and are responsible for the mineralization. The Sb deposition due to magmatism in central-north mainland Greece (central Macedonia, Thessaly) was associated with a later tectonic phase. The age of the intrusions in Gerakario, Lachanas, and Pelion are of Pliocene age, i.e., much later than the Oligocene–Miocene back-arc extension, and the faults that facilitated emplacement of subvolcanic intrusions, and also host the Sb mineralization, also belong to the Pliocene–early Pleistocene tectonic phase. The continuous extension with its various directions [62,66], has locally thinned the Aegean crust, allowing extensional faulting to facilitate the rise of the magma. In Philadelphia, the only outcropping intrusions nearby are of Triassic age [98]. A younger magmatic chamber may be present at a depth which is accessible by the Pliocene tectonics. Therefore, the Sb mineralization in Greece can be chronologically divided into two zones: (i) a progressive from (late) Oligocene to late Miocene spanning the eastern Greek territory (Thrace and east Aegean islands) associated directly with the back-arc extension following the Hellenic Arc's southward migration, and (ii) a quasi-simultaneous of Pliocene, spanning the central mainland Greece (central Macedonia, Thessaly) associated with a later extensional tectonic phase.

The antimony deposits in Greece originate from hydrothermal solutions with varying degrees of metal enrichment during mineralization. In some cases, the hydrothermal solutions exhibited significant differentiation, whereby several elements successively precipitated in the form of base metal ores, resulting in the final precipitation of almost monometallic antimony mineralization (stibnite and quartz). The aforementioned deposits are usually situated at a considerable distance from the magmatic source, resulting in the completion of hydrothermal solution differentiation, such as in the Lachanas deposit. Finally, there are other cases where the hydrothermal solutions are complex and undifferentiated and contain metals extracted from the host rocks through which they pass (or from magmas). In these cases, the antimony is precipitated in the form of stibnite and Sb-Pb sulfide minerals, such as the Kallintiri deposit.

Consequently, several antimony deposits in Greece exhibit significant characteristics, making the need for further research imperative since the potential for economically beneficial exploitation of these deposits is very possible. In any scenario, it is imperative that all endeavors towards exploration and exploitation be conducted based on societal consensus, based on a comprehensive understanding of the environment, and a strong commitment to ensuring the protection of the environment and the implementation of sustainable development strategies.

Table 1. Summary of the geological and mineralization characteristics of the antimony deposits of Greece.

Location	Possible Related Magmatism	Tectonic Setting during the Mineralization Deposition	Characteristics of the Mineralization	Geotectonic Zone
Kallintiri (Rhodope, NE Greece)	Late Eocene to Early Oligocene volcanic rock (andesite)	Ductile to brittle–ductile extensional deformation, low-angle normal detachment faults (D1, Oligocene)Brittle transpressional deformation, WNW-ESE/NW-SE strike-slip faults (D2, Late Oligocene)	Hydrothermal origin, controlled by tectonic processes. The ore mineralization stages are: Stage I: sph *, py *, gn *, fb-ttr *,qtz Stage II: zkn*, bnn*, gn, Pb-Sb sulfosalts [e.g., pgi *, Fül *], Stage III: sbn *, zkn *, Pb-Sb sulfosalts, qtz, cal Stage IV: sbn, sbr, bou, rlg, As(?), qtz, brt, dck	Rhodope massifCircum-Rhodope
Lachanas (Central Macedonia, Northern Greece)	Pliocene volcanic rocks (rhyolite, dacite and rhyodacite)	Brittle extensional deformation, ENE-WSW/NE-SW normal faults (Pliocene—Early Pleistocene)	Hydrothermal origin, controlled by tectonic processes. The ore mineralization stages are: Stage I: wf *, py *, apy * Stage II: sbn*, wf, py, As, ccp, Au	Serbomacedonian
Philadelphia (Central Macedonia, Northern Greece)	Pliocene volcanic rocks (rhyolite, dacite and rhyodacite)	Brittle extensional deformation, ENE-WSW/NE-SW normal faults (Pliocene—Early Pleistocene)	Hydrothermal origin, controlled by tectonic processes. The ore mineralization stages are: Stage I: sph *, py *, ttr *, apy *, qtz * Stage II: sbn *, ccsb *, ttr, py, apy, znk(?), qtz Stage III: py, znk, kem *, Au *, qtz, clay	Serbomacedonian
Gerakario (Central Macedonia, N. Greece)	Pliocene volcanic rocks (rhyolite and dacite)	Brittle extensional deformation, ENE-WSW/NE-SW normal faults (Pliocene–Early Pleistocene)	Hydrothermal origin, controlled by tectonic processes. The ore mineralization stages are: Stage I: apy *, btr *, Sb *, sbn, ccp(?), pyh, lol, qtz Stage II: sbn *, mrc *, py *, apy, Sb, ccp(?), Au, qtz Stage III: sbn *, Au *, py, mrc, qtz	Serbomacedonian
Chios Island (Aegean Sea, Eastern Greece)	Middle Miocene volcanic rocks (rhyolite)	Brittle deformation, N-S fault (unspecified age, possibly active until today)	Hydrothermal origin, controlled by tectonic processes. The ore mineralization stages are: Stage I: py *, sph *, ccp *, qtz *, ser Stage II: sbn *, py, ser *, cal *, qtz, Stage III: sbn *, py *	Pelagonian
Samos Island (Aegean Sea, Eastern Greece)	Upper Miocene volcanic rocks (mainly trachyte and rhyolite)	Ductile to brittle–ductile extensional deformation, low-angle normal detachment faults (D3, Middle–Late Miocene)Brittle deformation, NNE-SSW/NE-SW (D4, Late Miocene-Pliocene extension-parallel folding)	Hydrothermal origin, controlled by tectonic processes. The ore mineralization stages are: Stage I: sbn *, py *, mrc, qtz, flr, brt, ser, cal Stage II: py *, mrc, qtz, flr *, cal, gp(?)	Attico-Cycladic complex
Pelion (SE Thessaly, Central Greece)	Pliocene volcanic rocks (mainly diorite)	Brittle extensional deformation, ENE-WSW/NE-SW normal faults (Pliocene—Early Pleistocene)	Hydrothermal origin, controlled by tectonic processes. The ore mineralization stages are: Stage I: sph *, py *, apy *, qtz *, cal Stage II: sbn *, ccsb *, tnt *, cal *, qtz, dck Stage III: sbn, rlg, dck	Pelagonian

* = main mineral phase, **apy** = arsenopyrite, **As** = native As, **Au** = gold, **bnn** = bournonite, **bou** = boulangerite, **brt** = baryte, **btr** = berthierite, **btr** = berthierite, **cal** = calcite, **ccp** = chalcopyrite, **ccsb** = chalcostibite, **dck** = dickite, **fb** = freibergite, **flr** = fluorite, **fül** = fülöppite, **gn** = galena, **gp** = gypsum, **kem** = kermesite, **lol** = lolligite, **mrc** = marcasite, **pgi** = plagionite, **py** = pyrite, **pyh** = pyrrhotite, **qtz** = quartz, **rlg** = realgar, **Sb** = native Sb, **sbn** = stibnite, **sbr** = stibarsen, **ser** = sericite, **sph** = sphalerite, **tnt** = tennantite, **ttr** = tetrahedrite, **ttr** = tetrahedrite, **wf** = wolframite, **zkn** = zinkenite.

Author Contributions: Conceptualization, C.K.; methodology, C.K.; resources, C.K.; data curation, C.K., P.V., K.S. and S.S.; writing—original draft preparation, C.K.; writing—review and editing, C.K., S.S., P.V., K.S. and R.M.; visualization, C.K. and S.S.; funding acquisition, R.M. and C.K. All authors have read and agreed to the published version of the manuscript.

Funding: The corresponding author wishes to thank the Swiss Government for supporting the research economically through the program "Swiss Government Excellence Postdoctoral Scholarships 2013–2014".

Data Availability Statement: Data is contained within the article.

Conflicts of Interest: The authors declare no conflicts of interest.

References

1. European Commission, Directorate-General for Internal Market. Industry, Entrepreneurship and SMEs. In *Study on the Critical Raw Materials for the EU 2023—Final Report*; Grohol, M., Veeh, C., Eds.; Publications Office of the European Union: Luxembourg, 2023; Available online: https://data.europa.eu/doi/10.2873/725585 (accessed on 1 September 2023).
2. U.S. Congress. Consolidated Appropriations Act. 2021. Available online: https://rules.house.gov/sites/democrats.rules.house.gov/files/BILLS-116HR133SARCP-116-68.pdf (accessed on 4 March 2021).
3. Seal, R.R., II; Schulz, K.J.; DeYoung, J.H., Jr.; Sutphin, D.M.; Drew, L.J.; Carlin, J.F., Jr.; Berger, B.R. Antimony. In *Critical Mineral Resources of the United States—Economic and Environmental Geology and Prospects for Future Supply*; Schulz, K.J., DeYoung, J.H., Jr., Seal, R.R., II, Bradley, D.C., Eds.; Geological Survey Professional Paper 1802; U.S. Geological Survey: Reston, VA, USA, 2017; 19p, C1–C17. [CrossRef]
4. Lusty, P.A.J.; Shaw, R.A.; Gunn, A.G.; Idoine, N.E. *UK Criticality Assessment of Technology Critical Minerals and Metals*; British Geological Survey Commissioned Report, CR/21/120; British Geological Survey: Nottingham, UK, 2021; 76p.
5. Government of Canada. The Canadian Critical Minerals Strategy. From Exploration to Recycling: Powering the Green and Digital Economy for Canada and the World. Government of Canada. 2022. Available online: https://www.canada.ca/en/campaign/critical-minerals-in-canada/canadian-critical-minerals-strategy.html (accessed on 15 September 2023).
6. European Commission. Critical Raw Materials for the EU. European Commission. 2010. Available online: https://ec.europa.eu/growth/sectors/raw-materials/specific-interest/critical_en (accessed on 1 May 2023).
7. Miller, M.H. Antimony. In *United States Mineral Resources*; Brobst, D.A., Pratt, W.P., Eds.; U.S. Geological Survey Professional Paper 820; US Government Printing Office: Washington, DC, USA, 1973; pp. 45–50.
8. Rudnick, R.L.; Gao, S. *Composition of the Continental Crust, Treatise on Geochemistry*, 2nd ed.; Elsevier Ltd.: Amsterdam, The Netherlands, 2014. [CrossRef]
9. Eyi, E. *Antimony Uses, Production, Prices*; Tristar Resources plc: London, UK, 2012; p. 14.
10. Boyle, R.W.; Jonasson, I.R. The geochemistry of antimony and its use as an indicator element in geochemical prospecting. *J. Geochem. Explor.* **1984**, *20*, 223–302. [CrossRef]
11. Van den Brink, S.; Kleijn, R.; Sprecher, B.; Mancheri, N.; Tukker, A. Resilience in the antimony supply chain. *Resour. Conserv. Recycl.* **2022**, *186*, 106586. [CrossRef]
12. Mordor Intelligence. Market Snapshot. Mordor Intelligence. 2021. Available online: https://www.mordorintelligence.com/industry-reports/antimony-market (accessed on 15 September 2023).
13. Perpetua Resources. Antimony. A Critical Metalloid for Manufacturing, National Defense and the Next Generation of Energy Generation and Storage Technologies. Perpetua Resources. 2021. Available online: https://perpetuaresources.com/wp-content/uploads/Antimony-White-Paper.pdf (accessed on 1 February 2023).
14. Roskill. *Extract of Antimony: Global Industry, Markets and Outlook to 2028, 13th ed*; Roskill Information Services Ltd.: London, UK, 2018; 194p.
15. U.S. Geological Survey (USGS). *USGS Mineral Commodities Summary for 2023: Antimony*; USGS: Reston, VA, USA, 2023.
16. Carlin, J.F., Jr. *Antimony: U.S. Geological Survey Mineral Commodity Summaries 2011*; USGS: Reston, VA, USA, 2011; pp. 18–19. Available online: https://minerals.usgs.gov/minerals/pubs/commodity/antimony/mcs-2011-antim.pdf (accessed on 1 September 2022).
17. U.S. Geological Survey (USGS). *Mineral Commodity Summaries*; USGS: Reston, VA, USA, 2022. [CrossRef]
18. European Commission; Directorate-General for Internal Market, Industry, Entrepreneurship and SMEs; Blengini, G.; Cynthia, E.L.; Eynard, U.; De Matos Cristina, T.; Dominic, W.; Konstantinos, G.; Claudiu, P.; Samuel, C.; et al. *Study on the EU's List of Critical Raw Materials (2020)–Executive Summary*; Publications Office: Luxembourg, 2020; Available online: https://data.europa.eu/doi/10.2873/24089 (accessed on 1 February 2023).
19. Laznicka, P. Quantitative relationships among giant deposits of metals. *Econ. Geol.* **1999**, *94*, 455–473. [CrossRef]
20. Laznicka, P. *Giant Metallic Deposits—Future Sources of Industrial Metals*; Springer: Berlin, Germany, 2010; p. 834.
21. Guberman, D.E. *Antimony: U.S. Geological Survey Mineral Commodity Summaries 2014*; USGS: Reston, VA, USA, 2014; pp. 18–19. Available online: https://minerals.usgs.gov/minerals/pubs/commodity/antimony/mcs-2014-antim.pdf (accessed on 1 February 2023).

22. Schwarz-Schampera, U. Antimony. In *Critical Metals Handbook*; Gunn, G., Ed.; Wiley and Sons: Hoboken, NJ, USA, 2014; pp. 70–98. [CrossRef]
23. U.S. Geological Survey (USGS). *Mineral Commodities Summary for 2015: Antimony*; USGS: Reston, VA, USA, 2016.
24. Gibson, R.I. Type-cast—Antimony, the Metallic Sidekick, Sets the World on Fire and Puts it Out. Geotimes 1998, February, 58. Available online: https://www.gravmag.com/antimony.shtml (accessed on 1 September 2023).
25. Tercero Espinoza, L.; Hummen, T.; Brunot, A.; Pena Garay, I.; Velte, D.; Smuk, L.; Todorovic, J.; Eijk, C.; Joce, C. *CRM_InnoNet. Critical Raw Materials*; Substitution Profiles September 2013 Revised May 2015; European Commission: Brussels, Belgium, 2015; 96p.
26. Roskill. *The Economics of Antimony*, 10th ed.; Roskill Information Services Ltd.: London, UK, 2007; p. 231.
27. Wu, F.; Fu, Z.; Liu, B.; Mo, C.; Chen, B.; Corns, W.; Liao, H. Health risk associated with dietary co-exposure to high levels of antimony and arsenic in the world's largest antimony mine area. *Sci. Total Environ.* **2011**, *409*, 3344–3351. [CrossRef] [PubMed]
28. Rish, M.A. Antimony. In *Elements and their Compounds in the Environment—Occurrence, Analysis, and Biological Relevance*, 2nd ed.; Merian, E., Anke, M., Ihnat, M., Stoeppler, M., Eds.; Wiley-VCH Verlag: Weinheim, Germany, 2004; Chapter 4; pp. 659–670.
29. Obolensky, A.A.; Gushchina, L.V.; Borisenko, A.S.; Borovikov, A.A.; Pavlova, G.G. Antimony in hydrothermal processes. Solubility, conditions of transfer, and metal-bearing capacity of solutions. *Russ. Geol. Geophys.* **2007**, *48*, 992–1001. [CrossRef]
30. Pitcairn, I.K.; Teagle, D.A.; Craw, D.; Olivo, G.R.; Kerrich, R.; Brewer, T.S. Sources of metals and fluids in orogenic gold deposits—Insights from the Otago and Alpine schists, New Zealand. *Econ. Geol.* **2006**, *101*, 1525–1546. [CrossRef]
31. Hofstra, A.H.; Marsh, E.E.; Todorov, T.I.; Emsbo, P. Fluid inclusion evidence for a genetic link between simple antimony veins and giant silver veins in the Coeur d'Alene mining district, ID and MT, USA. *Geofluids* **2013**, *13*, 475–493. [CrossRef]
32. Hart, C.J.R. Reduced intrusion-related gold systems. In *Mineral deposits of Canada. A Synthesis of Major Deposit Types, District Metallogeny, the Evolution of Geological Priovinces, and Exploration Methods*; Goodfellow, W.D., Ed.; Special Publication No.5; Geological Association of Canada, Mineral Deposits Division: St. John's, NL, Canada, 2007; pp. 95–112.
33. Pohl, W.L. *Economic Geology: Principles and Practice*; Wiley Blackwell: Hoboken, NJ, USA, 2011.
34. Jankovic, S. The complex Antimony-Lead-Zink Deposit at Rujevac/Yugoslavia; its specific geochemical and mineralogical features. *Miner. Depos.* **1977**, *12*, 381–392. [CrossRef]
35. Jankovic, S. Antimony deposits in Southeastern Europe. *Veshik Geol.* **1979**, *37*, 25–48.
36. Mudrinic, C. The origin of the ore components and the geochemical characteristics of the antimony deposits of Serbia and Macedonia (Yugoslavia). In Proceedings of the Sixth Quadrennial IAGOD Symposium, Tbilisi, Georgia, 6–12 September 1982; E.Schweizerbart'sche: Stuttgart, Germany, 1984.
37. Dimou, E.; Papastaurou, S.; Serment, R. The antimony in Greece—Part I. In *Study of Occurrences and Deposits of Antimony in Northern Greece (Kallintiri, Philadelphia, Lachanas)*; IGME: Athens, Greece, 1985. (In Greek)
38. Robertson, A.H.F.; Dixon, J.E. Introduction. Aspects of the geological evolution of the Eastern Mediterranean. *Geol. Soc. Spec. Publ.* **1984**, *17*, 1–74. [CrossRef]
39. Şengör, A.M.C.; Yılmaz, Y.; Sungurlu, O. Tectonics of the Mediterranean Cimmerides. Nature and evolution of the western termination of Palaeo-Tethys. *Geol. Soc. Spec. Publ.* **1984**, *17*, 77–112. [CrossRef]
40. Robertson, A.H.F.; Dixon, J.E.; Brown, S.; Collins, A.; Morris, A.; Pickett, E.; Sharp, I.; Ustaömer, T. Alternative tectonic models for the Late Palaeozoic-Early Tertiary development of Tethys in the Eastern Mediterranean region. *Geol. Soc. Spec. Publ.* **1996**, *105*, 239–263. [CrossRef]
41. Mountrakis, D. Tertiary and Quaternary Tectonics of Greece. In *Postcollisional Tectonics and Magmatism in the Mediterranean Region and Asia*; Dilek, Y., Pavlides, S., Eds.; Geological Society of America: Boulder, CO, USA, 2006; Volume 409, pp. 125–136. [CrossRef]
42. Zulauf, G.; Dörr, W.; Fisher-Spurlock, S.C.; Gerdes, A.; Chatzaras, V.; Xypolias, P. Closure of the Paleo-Tethys in the External Hellenides. Constraints from U-Pb ages of magmatic and detrital zircons (Crete). *Gondwana Res.* **2015**, *28*, 642–667. [CrossRef]
43. Zulauf, G.; Dörr, W.; Marko, L.; Krahl, J. The late Eo-Cimmerian evolution of the external Hellenides. Constraints from microfabrics and U-Pb detrital zircon ages of Upper Triassic (meta)sediments (Crete, Greece). *Int. J. Earth Sci.* **2018**, *107*, 2859–2894. [CrossRef]
44. Laskari, S.; Soukis, K.; Stockli, D.F.; Lozios, S.; Zambetakis-Lekkas, A. Reconstructing the southern Pelagonian domain in the Aegean Sea. Insights from U-Pb detrital zircon analysis, lithostratigraphic and structural study, and zircon (U-Th)/He thermochronology on Amorgos Island (SE Cyclades, Greece). *Gondwana Res.* **2022**, *106*, 329–350. [CrossRef]
45. Dinter, D.A.; Royden, L. Late Cenozoic extension in northeastern Greece. Strymon Valley detachment system and Rhodope metamorphic core complex. *Geology* **1993**, *21*, 45–48. [CrossRef]
46. Gautier, P.; Brun, J.P.; Jolivet, L. Structure and kinematics of upper Cenozoic extensional detachment on Naxos and Paros (Cyclades Islands, Greece). *Tectonics* **1993**, *12*, 1180–1194. [CrossRef]
47. Gautier, P.; Brun, J.P. Crustal-scale geometry and kinematics of late-orogenic extension in the central Aegean (Cyclades and Ewia Island). *Tectonophysics* **1994**, *238*, 399–424. [CrossRef]
48. Sokoutis, D.; Brun, J.P.; Van Den Driessche, J.; Pavlides, S. A major Oligo-Miocene detachment in southern Rhodope controlling north Aegean extension. *J. Geol. Soc.* **1993**, *150*, 243–246. [CrossRef]

49. Kilias, A.; Falalakis, G.; Mountrakis, D. Cretaceous–Tertiary structures and kinematics of the Serbomacedonian metamorphic rocks and their relation to the exhumation of the Hellenic hinterland (Macedonia, Greece). *Int. J. Earth Sci.* **1999**, *88*, 513–531. [CrossRef]
50. Krohe, A.; Mposkos, E. Multiple generations of extensional detachments in the Rhodope Mountains (northern Greece). Evidence of episodic exhumation of high-pressure rocks. *Geol. Soc. Spec. Publ.* **2002**, *204*, 151–178. [CrossRef]
51. Jolivet, L.; Brun, J.P. Cenozoic geodynamic evolution of the Aegean. *Int. J. Earth Sci.* **2010**, *99*, 109–138. [CrossRef]
52. Jolivet, L.; Faccenna, C.; Piromallo, C. From mantle to crust. Stretching the Mediterranean. *Earth Planet. Sci. Lett.* **2009**, *285*, 198–209. [CrossRef]
53. Jolivet, L.; Faccenna, C.; Huet, B.; Labrousse, L.; Le Pourhiet, L.; Lacombe, O.; Lecomte, E.; Burov, E.; Denèle, Y.; Brun, J.P.; et al. Aegean tectonics. Strain localisation, slab tearing and trench retreat. *Tectonophysics* **2013**, *597*, 1–33. [CrossRef]
54. Jolivet, L.; Lecomte, E.; Huet, B.; Denèle, Y.; Lacombe, O.; Labrousse, L.; Le Pourhiet, L.; Mehl, C. The north cycladic detachment system. *Earth Planet. Sci. Lett.* **2010**, *289*, 87–104. [CrossRef]
55. Grasemann, B.; Schneider, D.A.; Stöckli, D.F.; Iglseder, C. Miocene bivergent crustal extension in the Aegean. Evidence from the western Cyclades (Greece). *Lithosphere* **2012**, *4*, 23–39. [CrossRef]
56. Grasemann, B.; Schneider, D.A.; Soukis, K.; Roche, V.; Hubmann, B. Paleogeographic position of the central Dodecanese Islands, southeastern Greece. The push-pull of Pelagonia. *GSA Bull.* **2022**, *134*, 1506–1528. [CrossRef]
57. Brun, J.P.; Sokoutis, D. Core complex segmentation in North Aegean, a dynamic view. *Tectonics* **2018**, *37*, 1797–1830. [CrossRef]
58. Schneider, D.A.; Grasemann, B.; Lion, A.; Soukis, K.; Draganits, E. Geodynamic significance of the Santorini Detachment System (Cyclades, Greece). *Terra Nova* **2018**, *30*, 414–422. [CrossRef]
59. Koukouvelas, I.; Doutsos, T. Tectonic stages along a traverse cross cutting the Rhodopian zone (Greece). *Geol. Rundsch.* **1990**, *79*, 753–776. [CrossRef]
60. Kokkalas, S.; Xypolias, P.; Koukouvelas, I. Structural evolution and kinematics in the contact zone between serbomacedonian and rhodope massifs, central Macedonia, Greece. *Bull. Geol. Soc. Greece* **2005**, *37*, 143–152.
61. Dinter, D.A. Late Cenozoic extension of the Alpine collisional orogen, northeastern Greece. Origin of the north Aegean basin. *Geol. Soc. Am. Bull.* **1998**, *110*, 1208–1230. [CrossRef]
62. Caputo, R.; Pavlides, S. Late Cainozoic geodynamic evolution of Thessaly and surroundings (central-northern Greece). *Tectonophysics* **1993**, *223*, 339–362. [CrossRef]
63. Kilias, A.; Falalakis, G.; Sfeikos, A.; Papadimitriou, E.; Vamvaka, A.; Gkarlaouni, C. The Thrace basin in the Rhodope province of NE Greece—A tertiary supradetachment basin and its geodynamic implications. *Tectonophysics* **2013**, *595*, 90–105. [CrossRef]
64. Mercier, J.L. Extensional-compressional tectonics associated with the Aegean Arc. Comparison with the Andean Cordillera of south Peru-north Bolivia. *Philos. Trans. R. Soc. Lond. Ser. A Math. Phys. Sci.* **1981**, *300*, 337–355.
65. Pavlides, S.B.; Kilias, A.A. Neotectonic and active faults along the Serbomacedonian zone (SE Chalkidiki, northern Greece). *Ann. Tectonicae* **1987**, *1*, 97–104.
66. Mercier, J.L.; Sorel, D.; Vergely, P.; Simeakis, K. Extensional tectonic regimes in the Aegean basins during the Cenozoic. *Basin Res.* **1989**, *2*, 49–71. [CrossRef]
67. Pavlides, S.; Mountrakis, D.; Kilias, A.; Tranos, M. The role of strike-slip movements in the extensional area of Northern Aegean (Greece). A case of transtensional tectonics. *Ann. Tecton.* **1990**, *4*, 196–211.
68. Taymaz, T.; Jackson, J.; McKenzie, D. Active tectonics of the north and central Aegean Sea. *Geophys. J. Int.* **1991**, *106*, 433–490. [CrossRef]
69. Armijo, R.; Meyer, B.; Hubert, A.; Barka, A. Westward propagation of the North Anatolian fault into the northern Aegean. Timing and kinematics. *Geology* **1999**, *27*, 267–270. [CrossRef]
70. Papanikolaou, D.; Alexandri, M.; Nomikou, P. Active faulting in the north Aegean basin. In *Postcollisional Tectonics and Magmatism in the Mediterranean Region and Asia*; Dilek, Y., Pavlides, S., Eds.; Geological Society of America: Boulder, CO, USA, 2006; Volume 409, pp. 189–209. [CrossRef]
71. Rodriguez, M.; Sakellariou, D.; Gorini, C.; Janin, A.; d'Acremont, E.; Pourhiet, L.L.; Chamot-Rooke, N.; Tsampouraki-Kraounaki, K.; Morfis, I.; Rousakis, G.; et al. Evolution of the North Anatolian Fault from a diffuse to a localized shear zone in the North Aegean Sea during the Plio-Pleistocene. *Geophys. J. Int.* **2023**, *235*, 2614–2639. [CrossRef]
72. Fytikas, M.; Innocenti, F.; Manetti, P.; Peccerillo, A.; Mazzuoli, R.; Villari, L. Tertiary to Quaternary evolution of volcanism in the Aegean region. *Geol. Soc. Spec. Publ.* **1984**, *17*, 687–699. [CrossRef]
73. Wilson, M.; Bianchini, G. Tertiary-Quaternary magmatism within the Mediterranean and surrounding regions. *Geol. Soc. Spec. Publ.* **1999**, *156*, 141–168. [CrossRef]
74. Pe-Piper, G.; Piper, D.J.W. Neogene backarc volcanism of the Aegean. New insights into the relationship between magmatism and tectonics. In *Cenozoic Volcanism in the Mediterranean Area*; Beccaluva, L., Bianchini, G., Wilson, M., Eds.; Geological Society of Amer: Boulder, CO, USA, 2007; pp. 17–31. [CrossRef]
75. Pe-Piper, G.; Piper, D.J.W. *The Igneous Rocks of Greece. The Anatomy of an Orogen: Beitrage zur ¨ Regionalen Geologie der Erde (Series)*; Springer: Berlin/Heidelberg, Germany, 2002.
76. Burg, J.P. Rhodope: From Mesozoic convergence to Cenozoic extension. Review of petro-structural data in the geochronological frame. *J. Virtual Explor.* **2012**, *42*, 1–44. [CrossRef]

77. Kilias, A.; Falalakis, G.; Sfeikos, A.; Papadimitriou, E.; Vamvaka, A.; Gkarlaouni, C. Architecture of Kinematics and Deformation History of the Tertiary Supradetachment Thrace Basin. Rhodope Province (NE Greece). In *New Frontiers in Tectonic Research—At the Midst of Plate Convergence*; Schattner, U., Ed.; IntechOpen: London, UK, 2011; pp. 241–268.
78. Bonev, N.; Beccaletto, L. From syn-to post-orogenic Tertiary extension in the north Aegean region. Constraints on the kinematics in the eastern Rhodope–Thrace, Bulgaria–Greece and the Biga Peninsula, NW Turkey. *Geol. Soc. Spec. Publ.* **2007**, *291*, 113–142. [CrossRef]
79. Brun, J.P.; Sokoutis, D. Kinematics of the southern Rhodope core complex (North Greece). *Int. J. Earth Sci.* **2007**, *96*, 1079–1099. [CrossRef]
80. Burchfiel, B.C.; Nakov, R.; Dumurdzanov, N.; Papanikolaou, D.; Tzankov, T.; Serafimovski, T.; King, R.W.; Kotzev, V.; Todosov, A.; Nurce, B. Evolution and dynamics of the Cenozoic tectonics of the South Balkan extensional system. *Geosphere* **2008**, *4*, 919–938. [CrossRef]
81. Zagorchev, I. Late Cenozoic development of the Strouma and Mesta fluviolacustrine systems, SW Bulgaria and northern Greece. *Quat. Sci. Rev.* **2007**, *26*, 2783–2800. [CrossRef]
82. Lybéris, N. Tectonic evolution of the North Aegean trough. *Geol. Soc. Spec. Publ.* **1984**, *17*, 709–725. [CrossRef]
83. Fountoulis, D. Etude Neotectonique et Seismotectonique du Bassin de Langadha (Macedoine, Grece). Ph.D. Thesis, Université Paris-Saclay, Paris, France, 1980; p. 185.
84. Jones, C.E.; Tarney, J.; Baker, J.H.; Gerouki, F. Tertiary granitoids of Rhodope, northern Greece. Magmatism related to extensional collapse of the Hellenic Orogen? *Tectonophysics* **1992**, *210*, 295–314. [CrossRef]
85. Koukouvelas, I.; Pe-Piper, G. The Oligocene Xanthi pluton, northern Greece. A granodiorite emplaced during regional extension. *J. Geol. Soc.* **1991**, *148*, 749–758. [CrossRef]
86. Kanellopoulos, C.; Voudouris, P.; Moritz, R. Detachment-related Sb-Pb-Zn-Ag-Au-Te mineralization in Kallyntiri area, northeastern Greece. Mineralogical and Geochemical constraints. *Bul. I Shk. Gjeol.* **2014**, *1/2014*, 162–165.
87. Michael, C.; Arvanitidis, N.D.; Iliadis, A.; Papavasileiou, K.; Christidis, C. Orogenic mineralizations—A new exploration target for gold-polymetallic ore deposits in Greece. In Proceedings of the 6th International Conference on Sustainable Development in the Minerals Industry, Milos Island, Greece, 30 June–3 July 2013; pp. 139–145.
88. Michael, C. *Research-Utilization Study Primary Gold*; IGME: Xanthi, Greece, 2002.
89. Stergiou, C.L.; Sakellaris, G.-A.; Melfos, V.; Voudouris, P.; Papadopoulou, L.; Kantiranis, N.; Skoupras, E. Mineralogy, Geochemistry and Fluid Inclusion Study of the Stibnite Vein-Type Mineralization at Rizana, Northern Greece. *Geosciences* **2023**, *13*, 61. [CrossRef]
90. Melidonis, N.G. *The Strymoniko-Metamorphosis Arc of Neo-Volcanic Rocks (Central Macedonia)*; Hellenic Survey of Geology and Mineral Exploration (HSGME): Athens, Greece, 1972; p. 51, (In Greek with German Abstract).
91. Kockel, F.; Mollat, H.; Antoniadis, P.; Ioannidis, K. *Geological Map of Greece. Sochos Map Sheet, 1.50,000*; IGME: Athens, Greece, 1979.
92. Institute of Geology and Mineral Exploration (IGME). *Geological Map of Greece, Scale 1.50,000, "Herson" Sheet*; IGME: Athens, Greece, 1990.
93. Tzamos, E.; Gamaletsos, P.N.; Grieco, G.; Bussolesi, M.; Xenidis, A.; Zouboulis, A.; Dimitriadis, D.; Pontikes, Y.; Godelitsas, A. New Insights into the Mineralogy and Geochemistry of Sb Ores from Greece. *Minerals* **2020**, *10*, 236. [CrossRef]
94. Stergiou, C.L.; Melfos, V.; Voudouris, P.; Papadopoulou, L.; Spry, P.G.; Peytcheva, I.; Dimitrova, D.; Stefanova, E. A Fluid Inclusion and Critical/Rare Metal Study of Epithermal Quartz-Stibnite Veins Associated with the Gerakario Porphyry Deposit, Northern Greece. *Appl. Sci.* **2022**, *12*, 909. [CrossRef]
95. Dimou, E.; Papastaurou, S.; Serment, R. The antimony in Greece-Part III. In *Study of Occurrences and Deposits of Antimony in Samos Island*; Kilkis, G., Rhodope, P., Chalkidiki, S., Eds.; IGME: Athens, Greece, 1987. (In Greek)
96. Himmerkus, F.; Reischmann, T.; Kostopoulos, D. Triassic rift-related meta-granites in the Internal Hellenides, Greece. *Geol. Mag.* **2009**, *146*, 252–265. [CrossRef]
97. Institute of Geological and Mining Research (IGMR). *Geological Map of Greece, Scale 1.50,000, "Zangliverion" Sheet*; IGSR: Athens, Greece, 1978.
98. Institute of Geological and Mining Research (IGMR). *Geological Map of Greece, Scale 1.50,000, "Sochos" Sheet*; IGSR: Athens, Greece, 1979.
99. Besenecker, H.; Dürr, S.; Herget, G.; Jacobshagen, V.; Kauffmann, G.; Lüdtke, G.; Roth, W.; Tietze, K.W. Geologie von Chios (Ägäis). *Geol. Palaeontol.* **1968**, *2*, 121–150.
100. Jacobshagen, V. Geologie von Griechenland. In *Beiträge Zur Regionalen Geologie der Erde Band 19*; Gebrüder Borntraeger: Berlin, Germany, 1986; 363p.
101. Robertson, A.H.; Pickett, E.A. Palaeozoic-Early Tertiary Tethyan evolution of mélanges, rift and passive margin units in the Karaburun Peninsula (western Turkey) and Chios Island (Greece). *Geol. Soc. Spec. Publ.* **2000**, *173*, 43–82. [CrossRef]
102. Robertson, A.H.; Ustaömer, T. Upper Palaeozoic subduction/accretion processes in the closure of Palaeotethys. Evidence from the Chios Melange (E Greece), the Karaburun Melange (W Turkey) and the Teke Dere Unit (SW Turkey). *Sediment. Geol.* **2009**, *220*, 29–59. [CrossRef]

103. Stampfli, G.M.; Vavassis, I.; De Bono, A.; Rosselet, F.; Matti, B.; Bellini, M. Remnants of the Paleotethys oceanic suture-zone in the western Tethyan area. Stratigraphic and structural evolution on the Late Carboniferous to Triassic continental and marine successions in Tuscany (Italy). Regional reports and general correlation. *Boll. Soc. Geol. Ital.* **2003**, *2*, 1–24.
104. Zanchi, A.; Garzanti, E.; Larghi, C.; Angiolini, L.; Gaetani, M. The Variscan orogeny in Chios (Greece). Carboniferous accretion along a Palaeotethyan active margin. *Terra Nova* **2003**, *15*, 213–223. [CrossRef]
105. Meinhold, G.; Kostopoulos, D.; Reischmann, T. Geochemical constraints on the provenance and depositional setting of sedimentary rocks from the islands of Chios, Inousses and Psara, Aegean Sea, Greece. Implications for the evolution of Palaeotethys. *J. Geol. Soc.* **2007**, *164*, 1145–1163. [CrossRef]
106. Meinhold, G.; Reischmann, T.; Kostopoulos, D.; Lehnert, O.; Matukov, D.; Sergeev, S. Provenance of sediments during subduction of Palaeotethys. Detrital zircon ages and olistolith analysis in Palaeozoic sediments from Chios Island, Greece. *Palaeogeogr. Palaeoclimatol. Palaeoecol.* **2008**, *263*, 71–91. [CrossRef]
107. Groves, J.R.; Larghi, C.; Nicora, A.; Rettori, R. Mississippian (Lower Carboniferous) microfossils from the Chios Mélange (Chios Island, Greece). *Geobios* **2003**, *36*, 379–389. [CrossRef]
108. Institute for Geology and Subsurface Research (IGSR). *Geological Map of Greece, Scale 1.50,000, "Chios" Sheet*; IGSR: Athens, Greece, 1971.
109. Herget, G.; Roth, W. Stratigraphie des Paläozoikums im Nordwest-Teil der Insel Chios (Ägäis). *Neues Jahrb. Für Geol. Und Paläontologie Abh.* **1968**, *131*, 46–71.
110. Pe-Piper, G.; Piper, D.J.W.; Kotopouli, C.N.; Panagos, A.G. Neogene volcanoes of Chios, Greece. The relative importance of subduction and back-arc extension. *Geol. Soc. Spec. Publ.* **1994**, *81*, 213–231. [CrossRef]
111. Bellon, H.; Grissollet, G.; Sorel, D. Age de l' activè volcanique Nèogène de l'île de Chios (Mer Egèe, Grece). *C. R. Acad. Sci. Paris.* **1979**, *288*, 1255–1258.
112. Chatzipetros, A.; Kiratzi, A.; Sboras, S.; Zouros, N.; Pavlides, S. Active faulting in the north-eastern Aegean Sea Islands. *Tectonophysics* **2013**, *597*, 106–122. [CrossRef]
113. Ring, U.; Laws, S.; Bernet, M. Structural analysis of a complex nappe sequence and late-orogenic basins from the Aegean Island of Samos, Greece. *J. Struct. Geol.* **1999**, *21*, 1575–1601. [CrossRef]
114. Bozkurt, E.; Park, L.R. Southern Menderes Massif. An incipient metamorphic core complex in western Anatolia, Turkey. *J. Geol. Soc.* **1994**, *151*, 213–216. [CrossRef]
115. Gessner, K.; Ring, U.; Güngör, T. *Field Guide to Samos and the Menderes Massif. Along-Strike Variations in the Mediterranean Tethyan Orogen*; Field Guide 23; Geological Society of America: Boulder, CO, USA, 2011; p. 52.
116. Gessner, K.; Ring, U.; Johnson, C.; Hetzel, R.; Passchier, C.W.; Güngör, T. An active bivergent rolling-hinge detachment system. Central Menderes metamorphic core complex in western Turkey. *Geology* **2001**, *29*, 611–614. [CrossRef]
117. Işik, V.; Tekeli, O. Late orogenic crustal extension in the northern Menderes massif (western Turkey). Evidence for metamorphic core complex formation. *Int. J. Earth Sci.* **2001**, *89*, 757–765. [CrossRef]
118. Altinok, Y.; Alpar, B.; Özer, N.; Gazioglu, C. 1881 and 1949 earthquakes at the Chios-Cesme Strait (Aegean Sea) and their relation to tsunamis. *Nat. Hazards Earth Syst. Sci.* **2005**, *5*, 717–725. [CrossRef]
119. Ocakoğlu, N.; Demirbağ, E.; Kuşçu, İ. Neotectonic structures in İzmir Gulf and surrounding regions (western Turkey). Evidences of strike-slip faulting with compression in the Aegean extensional regime. *Mar. Geol.* **2005**, *219*, 155–171. [CrossRef]
120. Emre, Ö.; Duman, T.Y.; Özalp, S.; Şaroğlu, F.; Olgun, Ş.; Elmacı, H.; Çan, T. Active fault database of Turkey. *Bull. Earthq. Eng.* **2018**, *16*, 3229–3275. [CrossRef]
121. Dimou, E.; Papastaurou, S.; Serment, R. *The Antimony in Greece-Part II. Study of Occurrences and Deposits of Antimony in Chios Island and Pelion*; IGME: Athens, Greece, 1986. (In Greek)
122. Skarpelis, N. Epithermal type ores in the Aegean. The hot spring minearalisation of northern Chios Island, Greece. *Bull. Geol. Soc. Greece* **1999**, *33*, 61–68.
123. Institute of Geological and Mining Research (IGMR). *Geological Map of Greece, Scale 1.50,000, "Samos Island" Sheet*; IGSR: Athens, Greece, 1979.
124. Papanikolaou, D. Unités tectoniques et phases de déformation dans l'île de Samos, Mer Egée, Grèce. *Bull. Soc. Géol. Fr.* **1979**, *S7-XXI*, 745–752. [CrossRef]
125. Roche, V.; Jolivet, L.; Papanikolaou, D.; Bozkurt, E.; Menant, A.; Rimmelé, G. Slab fragmentation beneath the Aegean/Anatolia transition zone. Insights from the tectonic and metamorphic evolution of the Eastern Aegean region. *Tectonophysics* **2019**, *754*, 101–129. [CrossRef]
126. Pe-Piper, G.; Piper, D.J.W. Late Miocene igneous rocks of Samos. The role of tectonism in petrogenesis in the southeastern Aegean. *Geol. Soc. Spec. Publ.* **2007**, *291*, 75–97. [CrossRef]
127. Earthquake Planning and Protection Organization (EPPO). *Neotectonic Map of Greece, Scale 1.75,000, "Samos" Sheet*; EPPO: Athens, Greece, 2006.
128. Sboras, S.; Lazos, I.; Bitharis, S.; Pikridas, C.; Galanakis, D.; Fotiou, A.; Chatzipetros, A.; Pavlides, S. Source modelling and stress transfer scenarios of the October 30, 2020 Samos earthquake. Seismotectonic implications. *Turk. J. Earth Sci.* **2021**, *30*, 699–717. [CrossRef]
129. Institute of Geology and Mineral Exploration (IGME). *Geological Map of Greece, Scale 1.50,000, "Zagora-Syki" Sheet*; IGME: Athens, Greece, 1987.

130. Tataris, A.A. Volcanic dykes and mineralization of the Mt. Pelion, Thessaly. In *Geological and Geophysical Research*, 4th ed.; Institute for Geology and Subsurface Research: Athens, Greece, 1960; (In Greece, with English Summary).
131. Lacassin, R.; Arnaud, N.; Leloup, P.-H.; Armijo, R.; Meyer, B. Synand post-orogenic exhumation of metamorphic rocks in North Aegean. *eEarth* **2007**, *2*, 51–63. [CrossRef]
132. Galanakis, D. Neotectonic and Stratihraphic of the Neogene-Quaternary Sediments of Almyros-Pagasitikos, Pilio, Oreoi-Trikeri and Maliakos Basins. Ph.D. Thesis, Aristotle University of Thessaloniki, Thessaloniki, Greece, 1997. (In Greek, with English Abstract).
133. Michael, C.; Constantinides, D.; Ashworth, K.; Peridikatsis, V. The polymetallic mineralization of the Pefka area, Evros country. Greece. *Geol. Rhodopica* **1989**, *1*, 366–373.
134. Voudouris, P. Te-rich magmatic-hydrothermal systems in northeastern Greece. *Mineral. Petrol.* **2006**, *87*, 241–275. [CrossRef]
135. Voudouris, P.; Mavrogonatos, C.; Spry, P.G.; Baker, T.; Melfos, V.; Klemd, R.; Haase, K.; Repstock, A.; Djiba, A.; Bismayer, U.; et al. Porphyry and epithermal deposits in Greece. An overview, new discoveries, and mineralogical constraints on their genesis. *Ore Geol. Rev.* **2019**, *107*, 654–691. [CrossRef]
136. Voudouris, P.; Repstock, A.; Spry, P.G.; Frenzel, M.; Mavrogonatos, C.; Keith, M.; Tarantola, A.; Melfos, V.; Tombros, S.; Zhai, D.; et al. Physicochemical constraints on indium-, tin-, germanium-, gallium-, gold-, and tellurium-bearing mineralizations in the Pefka and St Philippos polymetallic vein- and breccia-type deposits, Greece. *Ore Geol. Rev.* **2022**, *140*, 104348. [CrossRef]
137. Siron, C.R.; Baker, T. Overview of the Kassandra mining district, Halkidiki Peninsula, northern Greece. *Soc. Econ. Geol. Guideb. Ser.* **2016**, *54*, 113–127.
138. Siron, C.R.; Thompson, J.F.H.; Baker, T.; Friedman, R.; Tsitsanis, P.; Russell, S.V.; Randall, S.B.; Mortensen, J.K. Magmatic and metallogenic framework of Au-Cu porphyry and polymetallic carbonate-hosted replacement deposits of the Kassandra mining district, Northern Greece. *Soc. Econ. Geol. Spec. Publ.* **2016**, *19*, 29–55.
139. Voudouris, P.; Melfos, V.; Spry, P.G.; Bonsall, T.; Tarkian, M.; Economou-Eliopoulos, M. Mineralogy and fluid inclusion constraints on the evolution of the Plaka intrusion-related ore system, Lavrion, Greece. *Mineral. Petrol.* **2008**, *93*, 79–110. [CrossRef]
140. Voudouris, P.; Melfos, V.; Spry, P.G.; Bonsall, T.A.; Tarkian, M.; Solomos, C. Carbonate-replacement Pb-Zn-Ag±Au mineralization in the Kamariza area, Lavrion, Greece. Mineralogy and thermochemical conditions of formation. *Mineral. Petrol.* **2008**, *94*, 85–106. [CrossRef]
141. Bonsall, T.A.; Spry, P.G.; Voudouris, P.; Seymour, K.S.; Tombros, S.; Melfos, V. The Geochemistry of Carbonate-Replacement Pb-Zn-Ag Mineralization in the Lavrion District, Attica, Greece. Fluid Inclusion, Stable Isotope, and Rare Earth Element Studies. *Econ. Geol.* **2011**, *106*, 619–651. [CrossRef]
142. Scheffer, C.; Tarantola, A.; Vanderhaeghe, O.; Voudouris, P.; Spry, P.G.; Rigaudier, T.; Photiades, A. The Lavrion Pb-Zn-Ag-rich Vein and Breccia Detachment-Related Deposits (Greece). Involvement of Evaporated Seawater and Meteoric Fluids during Post-Orogenic Exhumation. *Econ. Geol.* **2019**, *114*, 1415–1442. [CrossRef]
143. Voudouris, P.; Melfos, M.; Mavrogonatos, C.; Photiades, A.; Moraiti, E.; Rieck, B.; Kolitsch, U.; Tarantola, A.; Scheffer, C.; Morin, D.; et al. The Lavrion mines. A unique site of geological and mineralogical heritage. *Minerals* **2021**, *11*, 76. [CrossRef]
144. Baumgärtl, U.; Burow, J. Laurion. *Aufschluss* **2002**, *53*, 245–362.
145. Solomos, C.; Voudouris, P.; Katerinopoulos, A. Mineralogical study of bismuth-gold–antimony mineralization at the area of Kamariza, Lavrion. *Bull. Geol. Soc. Greece* **2004**, *36*, 387–396. [CrossRef]
146. Ottens, B.; Voudouris, P. *Griechenland. Mineralien-Fundorte-Lagerstätten*; Christian Weise Verlag: Munchen, Germany, 2018; p. 480. ISBN 978-3-921656-86-0.
147. Institute of Geology and Mineral Exploration (IGME). *Geological Map of Greece; Scale 1.50,000, "Velestino" Sheet*; IGME: Athens, Greece, 1983.
148. Dimou, E. Sulfide occurrences in the serpentinites—Chromites in the Eretria area. *Bull. Geol. Soc. Greece* **1991**, *25*, 337–353.
149. Caputo, R. *Geological and Structural Study of the Recent and Active Brittle Deformation of the Neogene-Quaternary Basins of Thessaly (Greece)*; Scientific Annals, 12; Aristotle University of Thessaloniki: Thessaloniki, Greece, 1990; p. 252.
150. Kanellopoulos, C.; Mitropoulos, P.; Valsami-Jones, E.; Voudouris, P. A new terrestrial active mineralizing hydrothermal system associated with ore-bearing travertines in Greece (northern Euboea Island and Sperchios area). *J. Geochem. Explor.* **2017**, *179*, 9–24. [CrossRef]
151. Kanellopoulos, C.; Xenakis, M.; Vakalopoulos, P.; Kranis, H.; Christopoulou, M.; Vougioukalakis, G. Seawater-dominated, tectonically controlled and volcanic related geothermal systems. The case of the geothermal area in the northwest of the island of Euboea (Evia), Greece. *Int. J. Earth Sci.* **2020**, *109*, 2081–2112. [CrossRef]
152. Kanellopoulos, C.; Valsami-Jones, E.; Voudouris, P.; Stouraiti, C.; Moritz, R.; Mavrogonatos, C.; Mitropoulos, P. A new occurrence of terrestrial native iron in the earth's surface. The Ilia thermogenic travertine case, northwestern Euboea, Greece. *Geosci. J.* **2018**, *8*, 287. [CrossRef]
153. Kanellopoulos, C.; Thomas, C.; Xirokostas, N.; Ariztegui, D. Banded Iron Travertines at the Ilia Hot Spring (Greece). An interplay of biotic and abiotic factors leading to a modern BIF analog? *Depos. Rec.* **2019**, *5*, 109–130. [CrossRef]

154. Sheldon, H.A.; Micklethwaite, S. Damage and permeability around faults. Implications for mineralization. *Geology* **2007**, *34*, 903–906. [CrossRef]
155. Micklethwaite, S.; Sheldon, H.A.; Baker, T. Active fault and shear processes and their implications for mineral deposit formation and discovery. *J. Struct. Geol.* **2010**, *32*, 151–165. [CrossRef]

Disclaimer/Publisher's Note: The statements, opinions and data contained in all publications are solely those of the individual author(s) and contributor(s) and not of MDPI and/or the editor(s). MDPI and/or the editor(s) disclaim responsibility for any injury to people or property resulting from any ideas, methods, instructions or products referred to in the content.